

General Disclaimer

One or more of the Following Statements may affect this Document

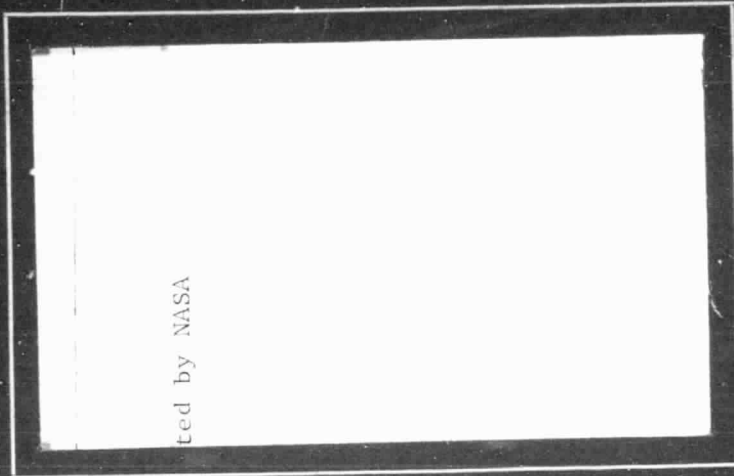
- This document has been reproduced from the best copy furnished by the organizational source. It is being released in the interest of making available as much information as possible.
- This document may contain data, which exceeds the sheet parameters. It was furnished in this condition by the organizational source and is the best copy available.
- This document may contain tone-on-tone or color graphs, charts and/or pictures, which have been reproduced in black and white.
- This document is paginated as submitted by the original source.
- Portions of this document are not fully legible due to the historical nature of some of the material. However, it is the best reproduction available from the original submission.

(NASA-CF-148296) DATA ACQUISITION AND PATH
SELECTION DECISION MAKING FOR AN AUTONOMOUS
ROVING VEHICLE Progress Report, 1 Jan. - 30
Jun. 1976 (Rensselaer Polytechnic Inst.)
46 p HC \$4.00

N76-27148

CSCI 03E G3/91

Unclas
44489



Rensselaer Polytechnic Institute

Troy, New York



A PROGRESS REPORT FOR
JANUARY 1, 1976 to JUNE 30, 1976

DATA ACQUISITION AND PATH SELECTION DECISION
MAKING FOR AN AUTONOMOUS ROVING VEHICLE

NATIONAL AERONAUTICS AND SPACE ADMINISTRATION
GRANT ~~7184~~ 7184
NSG-

D. K. Frederick
C. N. Shen
S. W. Yerazunis

RENSSELAER POLYTECHNIC INSTITUTE
TROY, NEW YORK

JULY 1, 1976



ABSTRACT

Problems related to the guidance of an autonomous rover for unmanned planetary exploration have been investigated. Included in these studies were: simulation on an interactive graphics computer system of the Rapid Estimation Technique for detection of discrete obstacles; incorporation of a simultaneous Bayesian estimate of states and inputs in the Rapid Estimation Scheme; development of methods for estimating actual laser rangefinder errors and their application to date provided by Jet Propulsion Laboratory; and modification of a path selection system simulation computer code for evaluation of a hazard detection system based on laser rangefinder data.

INTRODUCTION

A thorough exploration of planets or other extraterrestrial bodies by unmanned data acquisition systems must deal with formidable control problems posed by the long (9 to 45 minutes for Mars and more in other cases) round-trip communications delay. Time delays of these orders of magnitude preclude all but the most rudimentary and short range missions unless a high degree of automation is achieved. An augmented Viking mission or a sophisticated sample return program aspiring to the exploration of a region of 500-1000/cm diameter would require the availability of an autonomous rover requiring only occasional earth control.

In looking forward to detailed unmanned exploration of the planets, there are two prerequisites. First is the requirement that a high mobility rover or relocatable device be available. The higher the mobility (or capability of the device to deal with irregular and difficult terrain features), the more available will be the paths to the desired targets. A rover of low mobility may well find itself with no acceptable paths in many instances.

Second, a path selection system of capability comparable to the mobility must be available. By path selection system are implied: (a) the terrain sensor(s) which are to acquire the necessary terrain data, (b) the terrain modeler which is to process the acquired data with the goal of describing the terrain features, and (c) the path selection algorithm to determine the specific path to be followed towards the target. Unless the path selection system can take full advantage of the rover's terrain negotiating capabilities, such a mission will be made unnecessarily lengthy in time, or desired objectives will not be achieved, or, in the worst case, the rover will be immobilized when in fact passable paths are available. On the other hand, if the path selection system is insufficiently discriminating, the rover may follow a dangerous path with the risk of a catastrophic accident.

The research program described herein has been directed towards problems of path selection including data acquisition and processing, path selection algorithms and the corresponding integrated path selection systems.

The program involves two major tasks: (a) terrain and obstacle detection and interpretation and (b) path selection system simulation.

The task of terrain and obstacle detection and interpretation is aimed at investigating alternative procedures for using range-pointing angle data such as might be obtained from a laser rangefinder with the goal of detecting discrete obstacle hazards and/or impassable terrain contours. Included in the investigation are the effects of data density in space and time as well as of measurement errors inherent to the sensor and to the dynamical motion of the rover. A major emphasis is being directed to the mathematical processing of the data to reduce computational requirements and to increase the amount of useful information derived from the measurements. Although the study is aimed at the mid-range of 3 to 30 meters, it can be extended with very modest effort to longer ranges. Thus it could be used as the basis for optimization of long range path segments. The sub-tasks which have been

completed to date include implementation of the simulation of the Rapid Estimation Scheme on an interactive graphics computer system, development of the mathematical procedures for using a Bayesian Estimate of States and Inputs for obstacle detection and estimates of laser range-finder accuracy for Mars rover application. These studies are summarized briefly below and are described in more detail in the reprints of three papers which are included. Future work will be directed to the application and evaluation of these methods with respect to reducing data requirements while retaining performance levels.

The second major task, namely, path selection systems simulation and evaluation, has the objective of appraising the effectiveness of alternative integrated path selection systems including the sensor(s), terrain modeler and path selection systems with data errors due to the sensor and vehicle dynamics. The simulator is a digital computer code capable of generating three-dimensional terrains of a broad variety on which can be superimposed a wide range of discrete hazards. The simulation affords the opportunity to screen, evaluate and modify alternative concepts prior to implementation in hardware. To date, the simulation has been modified to reflect a laser range finder of the type required to employ the Rapid Estimation Scheme and the mathematics of the edge detection procedure. Consideration has been given to a path selection algorithm suitable to this type of data. The progress which has been made is detailed in a following section. Also appended is a paper describing the use of the simulation in evaluating a short range hazard detection system based on a triangulation concept which suggests the effectiveness of the procedure. This paper is based on work supported by NASA Grant NGL 33-018-091.

Task A. Terrain and Obstacle Detection and Interpretation

Task A.1. Simulation of Edge Enhancement Technique - K. L. Leung
Faculty Advisor: Prof. C. N. Shen

An edge enhancement technique for the detection of discrete obstacles such as boulders and craters using a Rapid Estimation Scheme in conjunction with a Kalman Filter has been developed. In order to increase the researcher's effectiveness in perceiving the effects of orientation, form of hazard, data spacing and sensor error on the obstacle detection concept, the technique has been programmed on the IDIOM/Varian Interactive Graphics Computer System. The Rapid Estimation Scheme not only is shown to be capable of detecting the top edges of boulders and the near edges of craters but along the bottom edges of boulders and the far edges of craters. The simulation is now an operational tool which will be used to explore the detection concept in detail. It is described in detail in a reprint of a paper which follows below.

PRESENTED AT THE SEVENTH ANNUAL CONFERENCE ON MODELING AND SIMULATION, PITTSBURGH, PA., April 1976 and Published in the Proceedings of the Conference

SIMULATION OF OBSTACLE DETECTION SCHEME FOR MARS TERRAIN USING MINICOMPUTER*

K. L. Leung and C. N. Shen**
Rensselaer Polytechnic Institute
Troy, New York 12181

ORIGINAL PAGE IS
OF POOR QUALITY

ABSTRACT

Simulation for detection of obstacles on Martian Terrain is achieved by a rapid estimation scheme on Varian Data 620/i computer with IDIOM display. Sufficient information can be obtained to recognize the near and far edges of pyramids, hemispherical craters or boulders, and the combination thereof.

INTRODUCTION

An autonomous roving vehicle is to be sent to Mars for future exploration^[1]. A laser rangefinder having an accuracy of ± 10 centimeters, will scan an area ahead of the rover. An obstacle detection scheme will therefore be needed to process these range data to obtain complete outlines of distinct objects.

One detection scheme that has been developed by Reed, Sanyal and Shen^[2] makes use of the four-directional Laplacian method. This scheme works well in detecting top edge of a boulder and near edge of a crater but it fails to detect the bottom edge of a boulder and the far edge of a crater. The scheme can only detect large jumps in ranges, but not large jumps in slopes.

The above scheme was simulated on both the IBM 360/67 computer and the Varian Data 620/i computer by Sher and Shen^[3]. On both computers, the range data were generated by a searching scheme and then Gaussian noise was added to the range data to simulate the actual range. In the simulation with the Varian Data computer, an IDIOM graphic cathod-ray tube was employed to display the parameters, the topview of obstacle layout and the results for edge image. A light pen was also used by the operator to interrupt the display and to change the parameters.

Another obstacle detection scheme was developed by R. V. Sonalkar and C. N. Shen^[4] which uses a Rapid Estimation Scheme^[5,6] (R.E.S.) in conjunction with Kalman Filter. In the simulation on the IBM 360/67 computer, their scheme was shown to work extremely well in detecting complete edges of

boulders, craters, and other obstacles.

OBJECTIVE

The objective is to evaluate the performance of the obstacle detection scheme on a minicomputer. This paper simulates the Sonalkar-Shen Obstacle Detection Scheme on the Varian Data 620/i computer, making use of Sher and Shen's display subroutines for parameter, topview, and edge image displays.

The reason for this simulation is two-fold. Firstly, this enables easy parameter changing with light pen and teletype. Topviews of obstacles and the resulting edge images can be seen and the differences observed. The operator will then change the parameters accordingly and repeat the simulation. This means that the simulation can be done adaptively.

Secondly, the possibility of implementing this scheme on a small computer such as the Varian Data must be ascertained.

EQUATIONS FOR OBSTACLE DETECTION

The range data are given by the matrix R with the following elements:

$$R = \begin{matrix} & \rightarrow j \\ \begin{matrix} \uparrow \\ i \end{matrix} & \begin{bmatrix} r_{m1} & \dots & r_{m2} & \dots & \dots & r_{mn} \\ r_{m-1,1} & \dots & r_{m-1,2} & \dots & \dots & r_{m-1,n} \\ \dots & \dots & \dots & r_{i+1,j} & \dots & \dots \\ \dots & \dots & \dots & r_{ij} & \dots & \dots \\ \dots & \dots & \dots & r_{i-1,j} & \dots & \dots \\ r_{11} & \dots & r_{12} & \dots & \dots & r_{1n} \end{bmatrix} \end{matrix} \quad (1)$$

where r_{ij} is the range data for the terrain, the length of the laser beam from the ground. The indices i and j indicate the location in the angle of elevation, θ_i , and azimuth angle, ϕ_j . The quantity r_{ij} is the sum of the actual distance between the transmitter and the point on the ground

* Research sponsored by NASA Grant, NSG-7184

** Professor-Electrical & Systems Engineering Dept.

and the Gaussian noise due to the inaccuracy of the laser rangefinder. Hence

$$r_{ij} = d_{ij} + v_{ij} \quad (2)$$

The range matrix R is processed both along all columns and across all rows. When processed vertically up a column, it is expected to detect jumps in both range and in slope, a two-dimensional state vector is defined. The first component is the range d_i and the second is the difference in successive range data ϵ_i (slope) where

$$\epsilon_i = d_{i+1} - d_i \quad (3)$$

The quantities ϵ_i , d_i , β are illustrated in Figure 1, θ is illustrated in Figure 2.

Along a column, the j index is held constant. The state equation is given as follows by omitting the index j.

$$x_{i+1} = F_i x_i + w_i + B u_k \delta_{ik} \quad (4)$$

The measurement model is:

$$r_{i+1} = H x_{i+1} + v_{i+1} \quad (5)$$

where

$$x_i = \begin{bmatrix} d_i \\ \epsilon_i \end{bmatrix}; \quad F_i = \begin{bmatrix} 1 & 1 \\ 0 & f_i \end{bmatrix}; \quad H = [1 \quad 0]$$

$$B = \begin{bmatrix} 0 \\ 1 \end{bmatrix}; \quad u_k = \text{Jump in } \epsilon_k \text{ due to an edge} \quad (6)$$

It can be shown that for a flat plane,

$$f_i = \frac{1 + \Delta\beta \tan \beta_i}{1 - 2\Delta\beta \cot \beta_i} \quad (7)$$

$$\text{Also } \delta_{ik} = \begin{cases} 1 & \text{for } i = k \\ 0 & \text{for } i \neq k \end{cases} \quad (8)$$

which is a Kronecker delta function.

Vectors w_i and v_i represent plant and measurement noise respectively. The quantity w_i accounts for the deviation of the model from the actual state equation. The quantity v_i accounts for error in the rangefinder.

RANGE DATA AND NOISE GENERATION

The surface of each obstacle within the scanned area is described by its own geometric equation

$$f(x, y, z) = 0 \quad (9)$$

If the point on the ground right underneath the laser mast is taken as the origin, then a level plane with no obstacle is described by $z=0$.

To determine the range reading with azimuth angle θ , and angle of elevation β_i , imagine a laser beam at these angles. The height H and (x,y) coordinates of a point on the beam a small distance away from the laser rangefinder is calculated and this height is compared with the height z of the terrain with the same (x,y) coordinates. If H is greater than z, then H of the point one increment down the beam is calculated and compared with z of the corresponding (x,y). The procedure is repeated until z is greater than H. Using a bisection

method, the (x,y) coordinates of the point where the beam hits the terrain is determined. If the height of this point is z^* and the height of the rangefinder is D, then the true range reading d_{ij} is given by

$$d_{ij} = (D - z^*) / \sin(\beta_i) \quad (10)$$

Note that if the beam does not hit any obstacle, $z^*=0$ and

$$d_{ij} = D / \sin \beta_i \quad (11)$$

These are illustrated in Figures 2 and 3.

CAPACITY OF MACHINE

The computing machine used in this simulation is the Varian Data 620/i. The memory of this computer when expanded, is a limiting 32767 words, or roughly 32K. The operating system used in this computer takes up about 4K. Hence the available memory is only 28K. For comparison, the memories required by the various programs are tabulated on Table 1.

	Sonalkar Shen on IBM 360/67	Sher- Shen on Varian	Lewng- Shen on Varian
Rapid Estimation Scheme	8K		
4-directional w/o Display		22K	
4-directional w/ Display		28K	
R.E.S. w/Display by combining Sonalkar and Sher			34K
R.E.S. w/Display after Improvement			27.5K

TABLE 1
The Memory Requirements of Various Programs

TECHNIQUES USED IN COMBINING THE PROGRAMS

The original Sonalkar-Shen program that simulates the Rapid Estimation Scheme was written in Fortran suitable for the IBM computer, which has a great deal of convenient features not found in the Varian computer. In order to run this program on the Varian machine, these convenient features must be changed to standard FORTRAN.

After the two programs are made compatible, the four-directional Laplacian obstacle detection part in the Sher-Shen program is taken out, and the Sonalkar-Shen program, i.e., The Rapid Estimation Scheme, is put in.

Each of the two original programs is very long by itself. After they are combined, the resultant program is too long and requires too much memory, 34K. Hence it must be improved by reusing some memory spaces after the numbers that are stored in these spaces are used. That is to say, two or more variables share the same memory space because they are stored in that space at different non-overlapping instances of time during the execution. This only accounts for a small amount of memory saved. The major reduction in the memory requirement is achieved by storing the noiseless range matrix and noisy range matrix in the same memory spaces. Moreover, the spaces set aside for the noise matrix

in the original program is eliminated. Hence the noise is added to the noiseless range reading as it is generated and the resulting noisy range reading is put back in the same space, therefore erasing the noiseless reading. Here memory saving does not come at no expense because the noiseless range matrix and noise matrix can be retrieved as two separated matrices from the noisy range matrix.

PROCEDURE OF SIMULATION

The IDIOM displays three separate pictures, the specification, the top view of the layout and the edge enhancement. If no interruption occurs in the display process, the Varian 620/i will use the initial parameters for all calculations. The light pen is used to interrupt the processing by pointing at the parameter that one desires to change. The new value of this parameter is entered through the teletype. The Varian 620/i will then use the new data and continue the processing. The picture on display can be replaced by another picture by pointing the light pen at the appropriate character.

The inputs to the computer are the dimensions and locations of the obstacles (the dimensions of the obstacles not used will be zero), the height and location of the laser rangefinder, the maximum and minimum azimuth angles, the maximum and minimum angles of elevation, and the standard deviation of the Gaussian noise used. The above input parameters have initial values as specified in Figure 4(a). They can be changed through the use of the light pen and the teletype.

With the input parameters, the program then displays the top view of the obstacle layout on the IDIOM. When the display is interrupted by the light pen, the program then calculates the range data using Eq.'s (10) and (11).

With the noisy range data and the noise covariance, the program processes the range data to detect the complete edges of the obstacles, using the Rapid Estimation Scheme, i.e., Eq.'s (1) through (8). Eleven cases are simulated. The values of the inputs for each case are shown in Table 2.

NUMERICAL RESULTS AND DISCUSSION

Eleven cases were simulated. Each case is a different combination of obstacle sizes, locations, and noise parameters. Some have single obstacle and some have multiple obstacles. For each case, the parameters, topview, and edge enhancement are displayed. The values of different parameters are shown in the parameter display. The layouts of the obstacles are shown in the topview displays and the edge enhancement results, i.e., the edge images, are shown in the edge enhancement displays. The parameters are chosen to illustrate the effects of the change of noise covariance, obstacle sizes, and the distance between obstacles and laser for use in the Rapid Estimation Scheme. Some of these eleven cases are shown in Figures 4-10.

In Figure 4(c), case No. 1, only the top edge of the 1 meter radius hemispherical boulder at 10 meters from the laser rangefinder (L.R.F.) can be

detected because the obstacle is too close to the L.R.F. and hence the signal-to-noise ratio (SNR) is small with 5 cm. noise standard deviation. In case No. 2, the noise standard deviation is increased to 10 cm. and everything else is the same as in case No. 1.

In Figure 5, case No. 3, the complete edge of the boulder at 20 m. from L.R.F. is detected for noise with standard deviation equal to 5 cm. In case No. 4 and case No. 5, the simulation is repeated for case No. 3, except that the noise standard deviation is now 10 cm. and 20 cm. respectively. The performance is very good. In Figure 6, case No. 6, the complete edge of a 1 m. radius hemispherical boulder at 30 m. from L.R.F. with a noise standard deviation of 5 cm. is detected. The edge enhancement result is better than that of the same boulder with the same noise at 20 m. from L.R.F. In case No. 7, the noise standard deviation σ_N is increased to 20 cm. In this case, the bottom edge is not so well defined. Case number 9 is a hemispherical crater with 1.5 m. radius at 12 m. from the rover, with σ_N equal to 5 cm. The far and near edges of the crater are detected but some noisy edges are picked up in the background.

Figure 7, case No. 8, is an equilateral pyramid of height 1 m. at 20 m. from the rover, with σ_N equal to 5 cm. and 10 cm. respectively. Here R.E.S. does not work too well. The top of the pyramid gets truncated.

Case No. 10 (Fig. 8) and case No. 11 respectively are multiple obstacles having a hemispherical boulder, a hemispherical crater, and a pyramid with their sizes and locations shown in the topview and parameter displays. The σ_N in case No. 10 and 11 are 5 cm. and 10 cm. respectively. Complete edges of all three obstacles are detected for the case with a smaller σ_N . For the case with a larger σ_N , the far edge of the crater and the bottom edge of the pyramid are not detected.

CONCLUSION

It can be concluded that the Rapid Estimation Scheme works very well in detecting complete edges of obstacles if the obstacles are far enough from the laser rangefinder (> about 15 meters) and the noise standard deviation is not too large (< about 10 cm. This scheme can still detect top edge of boulder and near edge of crater if the obstacles are too close and noise standard deviation is larger than 10 cm. Therefore, the Rapid Estimation Scheme is equivalent to or better than the four-directional Laplacian scheme in performance. However, the former scheme needs slightly more computation than the latter. Therefore, the R.E.S. extracts more information from the noisy range matrix if the slightly larger number of computation is allowable.

REFERENCES

1. Jet Propulsion Laboratory, "An Exploratory Investigation of a 1979 Mars Roving Vehicle Mission", JPL Reports, 1970.
2. M. Reed, P. Sanyal and C.N. Shen, "A Practical Obstacle Detection System for the Mars Rover",

- Proceedings of the Milwaukee Symposium on Automatic Control, Mar. 1974, Milwaukee, Wis.
- J. S. Sher and C.N. Shen, "Simulation of The Range Data and The Picture Enhancement Scheme For The Mars Rover", 1975 Computer Science Conference, University of Maryland.
 - R.V. Sonalkar and C.N. Shen, "Mars Obstacle Detection By Rapid Estimation Scheme From Noisy Laser Rangefinder Readings", Proceedings of the Milwaukee Symposium on Automatic Control, March 1975, Milwaukee, Wis. pp 291-296.
 - P. Sanyal and C.N. Shen, "Bayes Decision Rule for Rapid Detection and Adaptive Estimation Scheme with Space Applications", IEEE Transactions on Automatic Control Vol. AC-19, No. 3, June 1974, pp 228-231.
 - R.V. Sonalkar and C.N. Shen, "Rapid Estimation and Detection Scheme for Unknown Discretized Rectangular Inputs", IEEE Transactions on Automatic Control, Vol. AC-20, No.1, Feb. 1975.

TABLE 2 Values of Input Parameters

No.	Location (x,y) in Meters			Height of in Meters		Radius of in Meters			Angle in Degrees				Stand. Deviation of noise in cm.	shown in Fig.
	of Pyramid	of Boulder	of Crater	range-finder	Pyramid	Boulder	Crater	Max. Azimuth	Min. Azimuth	Max. Elevation	Min. Elevation			
1	(-1,0)	(0,10)	(1,0)	3.0	0.0	1.0	0.0	7.0	-7.0	19.6	10.0	5.0	4	
2	(-1,0)	(0,10)	(1,0)	3.0	0.0	1.0	0.0	7.0	-7.0	19.6	10.0	10.0	n.s.	
3	(-1,0)	(0,20)	(1,0)	3.0	0.0	1.0	0.0	4.0	-4.0	9.0	5.0	5.0	5	
4	(-1,0)	(0,20)	(1,0)	3.0	0.0	1.0	0.0	4.0	-4.0	9.0	5.0	10.0	n.s.	
5	(-1,0)	(0,20)	(1,0)	3.0	0.0	1.0	0.0	4.0	-4.0	9.0	5.0	20.0	n.s.	
6	(-1,0)	(0,30)	(1,0)	3.0	0.0	1.0	0.0	3.0	-3.0	6.6	3.0	5.0	6	
7	(-1,0)	(0,30)	(1,0)	3.0	0.0	1.0	0.0	3.0	-3.0	6.6	3.0	10.0	n.s.	
8	(0,20)	(-1,0)	(1,0)	3.0	1.0	0.0	0.0	4.3	-4.3	9.0	5.0	5.0	7	
9	(1,16)	(-1,18)	(0,12)	2.0	0.0	0.0	1.5	7.5	-7.5	11.3	2.3	5.0	n.s.	
10	(1,16)	(-1,18)	(0,12)	2.0	1.0	1.0	1.5	7.5	-7.5	11.3	2.3	5.0	8	
11	(1,16)	(-1,18)	(0,12)	2.0	1.0	1.0	1.5	7.5	-7.5	11.3	2.3	10.0	n.s.	

n.s. means 'not shown'

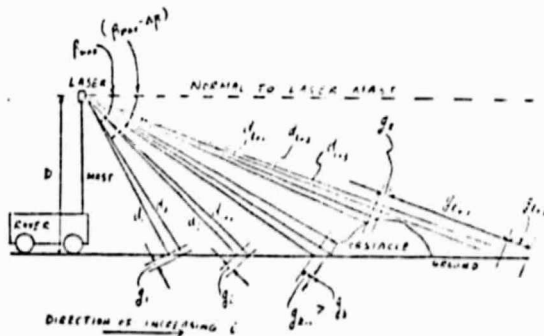


Figure 1 - Side View of Rover and Terrain

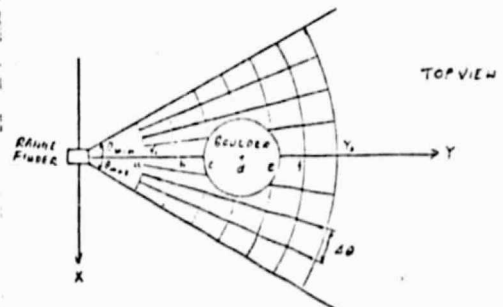
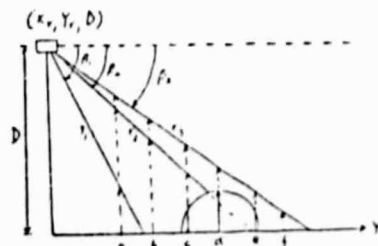


Figure 2-Rangefinder Scanning Scheme

Figure 3- Side View of the Plane with $\theta = 0^\circ$

RECOGNITION OF 3-D OBSTACLES AND A SIMULATION

STUDENT: HARSHAD LEUNG
PROFESSOR: P. M. C. W. SIEU

THIS PROGRAM SIMULATES THE EDGE DETECTION SCHEME
USED BY THE RANGE FINDER OF THE MARX ROVER

A PITCHED, A HEAD-SPHERE AND A CENTER ARE USED AS OBSTACLES

OBSTACLE SPECIFICATION:

1. LOCATION (X, Y) IN METERS

ROVER IS AT (0.0, 0.0)
PITCHED IS AT (1.0, 0.0)
HEAD-SPHERE IS AT (0.0, 10.0)
CENTER IS AT (1.0, 0.0)

Figure 4(a)
Parameter

2. SIZE IN METERS

HEIGHT OF THE PITCHED IS 7.0
HEIGHT OF THE CENTER IS 7.0
RADIUS OF THE HEAD-SPHERE IS 1.0
RADIUS OF THE CENTER IS 0.5

SCANNING RANGE AND NOISE:

1. HORIZONTAL SCAN COVERS 14.0 DEGREE

AND, FWHM = 7.0 DEGREE MIN. THETA = 17.0 DEGREE

2. VERTICAL SCAN COVERS 0.4 TO 17.0 M FROM THE ROVER

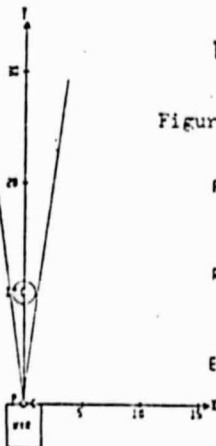
AND, DATA = 15.0 DEGREE MIN. DATA = 10.0 DEGREE

3. GAUSSIAN NOISE: MEAN VALUE 0.0 CM

STANDARD DEVIATION 5.0 CM

WESET TOPVIEW RANGE DATA EDGE DETECTION

0:00 ROVER
P: PITCHED
H: HEAD-SPHERE
C: CENTER



TOPVIEW

Figure 4(b)

PARAMETER

RNG. DATA

EDGE DET.

EDGE ENHANCEMENT BASED ON KALMAN FILTER & R.E.S.

COMPONENTS OF EDGE: 1 HORIZONTAL, 0 VERTICAL, 1 SHAPE, 1 0 CROSS

Figure 4(c)



PARAMETER TOPVIEW RANGE DATA

Display for Case #1

EDGE ENHANCEMENT BASED ON KALMAN FILTER & R.E.S.

COMPONENTS OF EDGE: 1 HORIZONTAL, 0 VERTICAL, 1 SHAPE, 1 0 CROSS

Figure 5
Display for
Case #3



PARAMETER TOPVIEW RANGE DATA

EDGE ENHANCEMENT BASED ON KALMAN FILTER & R.E.S.

COMPONENTS OF EDGE: 1 HORIZONTAL, 0 VERTICAL, 1 SHAPE, 1 0 CROSS

Figure 6
Display for
Case #6



PARAMETER TOPVIEW RANGE DATA

EDGE ENHANCEMENT BASED ON KALMAN FILTER & R.E.S.

COMPONENTS OF EDGE: 1 HORIZONTAL, 0 VERTICAL, 1 SHAPE, 1 0 CROSS

Figure 7
Display for
Case #8



PARAMETER TOPVIEW RANGE DATA

EDGE ENHANCEMENT BASED ON KALMAN FILTER & R.E.S.

COMPONENTS OF EDGE: 1 HORIZONTAL, 0 VERTICAL, 1 SHAPE, 1 0 CROSS

Figure 8
Display for
Case #10



PARAMETER TOPVIEW RANGE DATA

ORIGINAL PAGE IS
OF POOR QUALITY

Task A.2 Detection of Discrete Obstacles - R.V. Sonalkar
Faculty Advisor: Professor C. N. Shen

There are many potential methods which could conceivably be used to detect discrete obstacles on a terrain. The major objective of this task is to enhance the outlines of obstacles in a two-dimensional perspective view from a set of laser rangefinder data contaminated by measurement noise. A large discrete jump of the first differences of noisy rangefinder data will outline certain edges on obstacles (i.e. top and sides of a boulder and near edges of craters or crevasses). The Rapid Estimation Scheme can determine this jump of input under a sub-optimal condition by erasing all of the previous memory of the covariances of the Kalman Filter at the stage where the jump occurs. The present task has been aimed at retaining the past memory in the Kalman filter at the time during the estimation of the jump of the input and thus improve the estimate. The mathematical procedures required to achieve this objective have been developed and are described in detail in the reprint of the paper entitled "Simultaneous Bayesian Estimate of States and Inputs" which follows.

SIMULTANEOUS BAYESIAN ESTIMATION OF STATES AND INPUTS

R. V. Sonalkar, Member IEEE
PATTERN ANALYSIS AND RECOGNITION CORP.
On the Mall
Rome, New York 13440

C. N. Shen, Professor
Electrical and Systems Engineering Dept.
RENSSELAER POLYTECHNICAL INSTITUTE
Troy, New York 12181

ABSTRACT

This paper describes a Simultaneous Bayesian Estimate (SBE) of states and inputs. The discrete system under consideration is assumed to be subject to unknown inputs, isolated or repeated. The SBE is conditioned on the hypothesis that an input occurs. It is mainly designed to improve the Rapid Estimation Scheme (RES), [1,2] which relies upon getting a minimum variance (MV) input estimate. The SBE obtains an estimate of the input and also provides a proper correction to the existing state estimate, as opposed to the current RES which merely obtains a MV input estimate. The approach in RES was shown to be suboptimal in Ref. [1]. The SBE is proved to be existent under conditions which were imposed for obtaining the MV input estimate; i.e., it does not impose any more restrictions on the systems that may be considered, than the ones that already existed. Since the SBE is a conditional estimate, a decision scheme is required to determine if the unknown inputs are present. A Bayes decision rule used for such a purpose has been described in Ref. [1] and is not repeated in this paper.

NOMENCLATURE

Alphabetical Symbols

B	(nxq) Input distribution matrix
Cov(x)	Covariance matrix of the random variable x.
E(x)	Statistical expectation of x
F _i	(nxn) State transition or system dynamics matrix
H _i	(nxn) Measurement matrix
h	Hypothesis
I _n	(nxn) Identity matrix
k	First stage at which input occurs in a sequence
M _i	Covariance of the predicted state vector \hat{x}_i

n	Dimension of the state vector x_i
N(m, I)	Normal distribution with mean vector m and covariance matrix I
O _n	(nx1) Vector with all zero elements, n- null vector
P _i	Covariance of the state estimate \hat{x}_i
p(x/h)	pdf of x conditioned on h
q	Dimension of the input vector u_i
r	Last stage at which an input occurs in a sequence
R _i	(sxs) Observation noise covariance matrix
s	Dimension of the observation vector z_i
u _j	(qx1) Input vector
v _i	(sx1) WGN sequence vector
w _i	(nx1) WG plant or system noise sequence vector
x _i	(nx1) State vector
X _i	(n+q)x1 Augmented state vector
y ₁	nx1 Component vector
y ₂	qx1 Component vector
y	(n+q)x1 Joint vector of y ₁ and y ₂
z _i	(sx1) Observation vector

Greek Symbols

δ_{ij}	Kronecker delta function =1 if i=j and =0 if i≠j
Φ	Matrix defined by Eq. (24b), inverse of augmented state estimate covariance

- $\rho(A)$ Rank of matrix A
 Ψ Matrix defined by Eq. (8)

Subscripts

- i, j Time stage subscripts
 $n, n+q$ Dimensions of null-vectors 0.

Superscripts

- T Matrix transpose
 $*$ Quantity related to augmented system
 $1, 0$ Hypotheses

Special Symbols

- \hat{x}_i Best estimate of x_i
 \bar{x}_i Predicted estimate of x_i

Abbreviations

- KF Kalman filter
 MAP Maximum A Posteriori
 MV Minimum variance
 pdf Probability density function
 RES Rapid Estimation Scheme
 SBE Simultaneous Bayesian Estimate
 WGN White Gaussian Noise

INTRODUCTION

The applications of the Kalman filter have been extremely varied in numerous fields such as: satellite, aircraft, and ground vehicle tracking; feedback process control; image processing; edge detection; etc. The extensive use of the filter to obtain estimates of the states of a system has also manifested its shortcomings. The filter is optimal only if the system parameters are known correctly. On the other hand, uncertainties in the system dynamics and noise statistics often cause the filter to diverge, if no safeguards are introduced to detect and prevent such a runaway condition. Sudden changes in the states of a system, which may be encountered while tracking a maneuvering target, also result in throwing the filter off-track. These difficulties are increased when tracking multiple targets with multiple radars.

Such changes can be modelled as isolated inputs to the system [1,2] or sequences of inputs [2] added to the state. In general, the difference equation for the states of a system subject to unknown inputs can be written as follows: System dynamics:

$$x_{i+1} = F_i x_i + w_i + \sum_{j=k}^r B u_j \delta_{ij} \quad (1)$$

Observation equation:

$$z_{i+1} = H_{i+1} x_{i+1} + v_{i+1} \quad (2)$$

where x_i and w_i are n -vectors; u_j is an unknown q -vector; z_{i+1} and v_{i+1} are s -vectors; H_{i+1} , B , and F_i are known matrices of compatible dimensions. Vectors w_i and v_i are WGN sequence vectors. The plant noise vector w_i , the observation noise vector v_i , and the initial state x_0 are all assumed to be uncorrelated and of known distributions; the distributions being $N(0_n, Q_i \delta_{ij})$, $N(0_s, R_i \delta_{ij})$, and $N(x_0, P_0)$ respectively. Covariance Q_i is positive semi-definite while P_0 and R_i are positive definite matrices. Here, and in the subsequent derivations, 0_n denotes a null vector of dimension $(n \times 1)$, i.e., an n -vector with all zero elements.

In the absence of the input term, the state x_i could have been estimated optimally by the Kalman filter [4]. However, the presence of the unknowns u_j , k , and r in Eq. (1) pose the problem to be solved.

To detect such an input, it must be estimated at first. RES has used a suboptimal minimum variance input estimate which has been shown to exist if the following conditions are satisfied.

- a. $q \leq n \leq s$ (3a)
- b. Matrix (HB) is of full rank (3b)

The implications of these two conditions will be discussed in a later section.

It has also been shown in Ref. [5] that the MV input estimate is suboptimal since it is based on certain approximations. Under certain conditions the MV input estimate also causes the filter to lose its "memory" by basing the current state estimate entirely on the current observation.

Therefore, the advantage of having a smooth estimate until the input detection takes place, is lost and subsequent estimates are noisier.

In an effort to determine a better and possibly optimal joint state and input estimate, the method described in this paper was developed. The estimate retains the memory of the filter as opposed to the MV estimate which, under certain conditions, became a limited memory open-filter. The estimate has not been proved to be optimal, or even better than the previous MV estimate. However, because it has been derived from the basics without approximations, and because it retains the memory of the filter, it is expected that the simultaneous Bayesian estimate would provide a better filter performance.

The problem of detection is not described. The interested reader will find it in Refs. [1,2,5,6]. The SBE is derived, conditioned on the presence of the input. A decision scheme will have to be used in conjunction with this to determine whether this conditional estimate is correct.

BAYESIAN ESTIMATE

Two hypotheses are defined -

h^1 : Input occurs at stage i .

h^0 : Input does not occur at stage i .

These definitions assume that the decisions between stages 0 and $i-1$ have already been made.

$$\therefore h^1: x_{i+1}^1 = \Gamma_i x_i + w_i + B u_i \quad (4)$$

$$h^0: x_{i+1}^0 = \Gamma_i x_i + w_i \quad (5)$$

$$\therefore x_{i+1}^1 = x_{i+1}^0 + B u_i \quad (6)$$

Thus x_{i+1}^0 is the partial state without the input.

Defining a new augmented state X_{i+1} , Eq (6) can be rewritten in a new notation.

$$x_{i+1}^1 = [I_n \ B] \begin{bmatrix} x_{i+1}^0 \\ u_i \end{bmatrix} = \Psi X_{i+1} \quad (7)$$

$$\text{where } \Psi \triangleq [I_n \ B] ; X_{i+1} = \begin{bmatrix} x_{i+1}^0 \\ u_i \end{bmatrix} \quad (8)$$

I_n is a $(n \times n)$ unity matrix and X_{i+1} is the augmented $(n+q)$ vector. A priori information about x_{i+1}^0 exists in the form of the Kalman filter estimate at stage i .

$$\therefore E(x_{i+1}^0 | z_i) = \bar{x}_{i+1}^0 = F_i \hat{x}_i \quad (9)$$

where \hat{x}_i is the best unbiased estimate at stage i obtained from the observation z_i .

The error covariance of the unbiased a priori estimate \bar{x}_{i+1}^0 is obtained from the system dynamics, Eq. (1).

$$M_{i+1}^0 \triangleq E[(x_{i+1}^0 - \bar{x}_{i+1}^0)(x_{i+1}^0 - \bar{x}_{i+1}^0)^T / h^0] \\ = F_i P_i F_i^T + Q_i \quad (10)$$

$$\text{where } P_i \triangleq E[(x_i - \hat{x}_i)(x_i - \hat{x}_i)^T] \quad (11)$$

is the error covariance of the estimate \hat{x}_i .

Substituting Eq. (7) in (2), the observation equation conditioned on h^1 can be rewritten in a different form.

$$h^1: z_{i+1} = H_{i+1} x_{i+1}^1 + v_{i+1} \\ = H_{i+1}^* X_{i+1} + v_{i+1} \quad (12)$$

$$\text{where } H_{i+1}^* \triangleq H_{i+1} \Psi \quad (13)$$

and Ψ is defined by Eq. (8).

To obtain a MAP (maximum a posteriori) estimate of X_{i+1} , the probability density function (pdf) of X_{i+1} , conditioned on z_{i+1} , must be maximized. Using the Bayes rule for conditional probabilities [4]:

$$p(X_{i+1} / z_{i+1}) = \frac{p(z_{i+1} / X_{i+1}) p(X_{i+1})}{p(z_{i+1})} \quad (14)$$

Since, the state x_{i+1}^0 and input u_i are independent of each other, $p(X_{i+1})$ may be written as a product of $p(x_{i+1}^0)$ and $p(u_i)$.

$$\therefore p(X_{i+1} / z_{i+1}) = \frac{p(z_{i+1} / X_{i+1}) p(x_{i+1}^0) p(u_i)}{p(z_{i+1})} \quad (15)$$

We may consider u_i to be normally distributed, $N(\bar{u}_i, P_u)$ so that the derivative of $\ln p(u_i)$ with respect to X_i gives.

$$\frac{\partial \ln p(u_i)}{\partial X_i} = - \left(\frac{\partial u_i}{\partial X_i} \right)^T P_u^{-1} (u_i - \bar{u}_i) \quad (16)$$

The input vector u_i is assumed to be deterministic and of unknown magnitude. Therefore, it may be considered as a random variable with covariance tending to infinity. Allowing $P_u \rightarrow \infty$ causes $\frac{\partial \ln p(u_i)}{\partial X_i} \rightarrow 0_{n+q}$, [7]. This fact allows the maximization of $p(X_{i+1}/Z_{i+1})$ to be expressed in the following form.

$$\begin{aligned} \frac{\partial \ln p(X_{i+1}/Z_{i+1})}{\partial X_{i+1}} \Big|_{X_{i+1}} &= \left[\frac{\partial \ln p(z_{i+1}/X_{i+1})}{\partial X_{i+1}} \right. \\ &\left. + \frac{\partial \ln p(x_{i+1})}{\partial X_{i+1}} \right]_{X_{i+1}} = 0_{n+q} \quad (17) \end{aligned}$$

As is well known, the solution of this equation leads to the MAP estimate \hat{X}_{i+1} of the augmented state X_{i+1} .

It is understood that all the pdf's in Eq. (17) are conditioned on the previous observation z_i , which permits the pdf of x_i to be completely specified by its mean, Eq. (9), and covariance, Eq. (10). The conditional pdf $p(z_{i+1}/X_{i+1})$ requires the following quantities.

$$E(z_{i+1}/X_{i+1}) = H_{i+1}^* X_{i+1} \quad (18)$$

$$\text{Cov.}(z_{i+1}/X_{i+1}) = R_{i+1}$$

Before proceeding any further, let us suppress the subscripts for convenience and use the following notation.

$$\begin{aligned} x_{i+1}^0 &= x, & X_{i+1} &= X, & R_{i+1} &= R, & M_{i+1} &= M \\ u_i &= u, & z_{i+1} &= z, & H_{i+1}^* &= H^*, & H_{i+1} &= H \end{aligned} \quad (19)$$

For normally distributed variables, Eq. (17) can easily be shown to be reducible to the following minimization.

$$\frac{\partial}{\partial X} [(z-H^* X)^T R^{-1} (z-H^* X) + (x-\bar{x})^T M^{-1} (x-\bar{x})]_{X} = 0_{n+q} \quad (20)$$

Since $X = \begin{bmatrix} x \\ u \end{bmatrix}$, the minimization of the second term inside the parenthesis can be performed as follows:

$$\begin{aligned} \frac{\partial}{\partial X} [(x-\bar{x})^T M^{-1} (x-\bar{x})] &= \begin{bmatrix} \frac{\partial}{\partial x} \\ \frac{\partial}{\partial u} \end{bmatrix} [(x-\bar{x})^T M^{-1} (x-\bar{x})] \\ &= \begin{bmatrix} M^{-1} (x-\bar{x}) \\ 0_q \end{bmatrix} \quad (21) \end{aligned}$$

The last equality is due to the fact that x is independent of the input u . As a result, the term $\frac{\partial}{\partial u} [(x-\bar{x})^T M^{-1} (x-\bar{x})]$ is equal to the q -dimensional null vector, 0_q . Substituting Eq. (21) in (20)

$$\begin{aligned} \text{gives:} \\ -H^* T R^{-1} (z-H^* \hat{X}) + \begin{bmatrix} M^{-1} (\hat{x}-\bar{x}) \\ 0_q \end{bmatrix} &= 0_{n+q} \quad (22) \end{aligned}$$

By further manipulations, an expression for the Bayesian estimate \hat{X} is obtained.

$$\hat{X} = \bar{X} + \phi^{-1} H^* T R^{-1} (z-H^* \bar{X}) \quad (23)$$

$$\text{where } \bar{X} = \begin{bmatrix} \bar{x} \\ 0_q \end{bmatrix} = \begin{bmatrix} F_i^* \hat{x}_i^0 \\ 0_q \end{bmatrix} \quad (24a)$$

$$\phi = \left\{ H^* T R^{-1} H^* + \begin{bmatrix} M^{-1} & 0_{nq} \\ 0_{qn} & 0_{qq} \end{bmatrix} \right\} \quad (24b)$$

$$\text{and } \hat{X} = \begin{bmatrix} \hat{x} \\ \hat{u}_i \end{bmatrix} \quad (24c)$$

Even though similar in appearance, Eq. (23) bears differences in two striking details with the Kalman filter estimate. First, \bar{X} given by Eq. (24a) is not equal to $E(X) = \begin{bmatrix} E(x) \\ u \end{bmatrix}$ as is generally true in the Kalman filter updating equation. Secondly, the matrix ϕ is invertible only under

certain conditions to be derived below. In the KF equations, the error covariance P, which generally occurs in place of ϕ^{-1} , is positive definite by definition. On the other hand, SBE can be obtained only when ϕ is invertible when certain conditions are met.

Using Eqs. (8) and (13), the first term in Ψ is seen to be of the following form:

$$H^T R^{-1} H \Psi = \Psi^T H^T R^{-1} H \Psi = \begin{bmatrix} H^T R^{-1} H & H^T R^{-1} H B \\ \hline B^T H^T R^{-1} H & B^T H^T R^{-1} H B \end{bmatrix} \quad (25)$$

The matrix in Eq. (25) is of dimensions $[(n+q) \times (n+q)]$, but is of rank n . Since we have assumed $s > n$, R positive definite, and H to be of full rank, $H^T R^{-1} H$ is positive definite. Moreover, Ψ is a $[n \times (n+q)]$ matrix, given by Eq. (6), and is of full rank. Therefore, $\Psi^T H^T R^{-1} H \Psi$ cannot be of any higher rank than n .

$$\phi = \begin{bmatrix} H^T R^{-1} H & H^T R^{-1} H B \\ \hline B^T H^T R^{-1} H & B^T H^T R^{-1} H B \end{bmatrix} + \begin{bmatrix} M^{-1} & 0_{nq} \\ \hline 0_{qn} & 0_{qq} \end{bmatrix} \quad (26)$$

In Eq. (26), both matrices on the right side are positive semi-definite and of rank n each. Hence the rank of ϕ cannot be greater than $2n$. Let us see under what conditions, ϕ can be a positive definite matrix. If ϕ is to be positive definite, $y^T \phi y$ must be positive for any $(n+q)$ dimensional vector y , which does not have all zero elements.

If y is defined in terms of its n and q dimensional component vectors y_1 and y_2 respectively, i.e., if

$$y = \begin{bmatrix} y_1 \\ y_2 \end{bmatrix} \quad (27)$$

then, using Eq. (24b), $y^T \phi y$ may be written as follows:

$$y^T \phi y = y^T H^T R^{-1} H y + y_1^T M^{-1} y_1 \quad (28)$$

Therefore, if ϕ is to be positive definite, then

$$y^T H^T R^{-1} H y + y_1^T M^{-1} y_1 > 0 \quad (29)$$

must be satisfied for all $(n+q)$ dimensional vectors $y \neq 0_{n+q}$. Here $y \neq 0_{n+q}$ means that y is not equal to the null vector of $(n+q)$ dimensions, i.e., y has at least one non-zero element.

Any non-null vector y , defined by Eq. (27) can have either $y_1 = 0_n$ or $y_1 \neq 0_n$. Putting these two cases together, we cover all vectors y which are non-null, i.e., $y \neq 0_{n+q}$.

i) If $y_1 = 0_n$, then $y_2 \neq 0_q$; since $y_1 = 0_n$ and $y_2 = 0_q$ simultaneously will make $y = 0_{n+q}$, which must be excluded for proving (29). Now, inequality (29) reduces to the following after using Eq. (25).

$$y_2^T B^T H^T R^{-1} H B y_2 > 0 \quad (30)$$

If this inequality is to be true for all $y_2 \neq 0_q$ then $(HB)^T R^{-1} (HB)$, which is a $(q \times q)$ matrix, must be positive definite. This condition is satisfied if $q \leq n \leq s$ in addition to (HB) being a matrix of full rank. Matrices H and B are of dimensions $(s \times n)$ and $(n \times q)$ respectively, so that the $(s \times q)$ matrix (HB) must be of rank q . Therefore, inequality (30) is true for all $y_2 \neq 0_q$ if:

$$a) \quad q \leq n \leq s \quad \text{and} \quad b) \quad \text{Rank}(HB) = q$$

ii) When $y_1 \neq 0_n$, y_2 may take any value, since

$y \neq 0_{n+q}$ is satisfied by virtue of $y_1 \neq 0_n$.

Under this condition, inequality (29) remains unchanged. However, M^{-1} is positive definite, which makes $y_1^T M^{-1} y_1 > 0$ for all $y_1 \neq 0_n$. Therefore, the sum of two quantities, one of which is positive ($y_1^T M^{-1} y_1 > 0$) and the other non-negative ($y^T H^* T R^{-1} H^* y \geq 0$), must be positive. As a result, under this case also, inequality (28) is satisfied.

Putting these two cases together, the conditions to be satisfied for the positive definiteness of ϕ are:

- a) $q \leq n \leq s$: $\text{rank}(HB) = q$
 b) M^{-1} must be positive definite (31)

Conditions (31a) are the same as (3a) and (3b) which were the necessary conditions for obtaining the MV estimate in EES. Also, M is the error covariance of the KF predicted state \bar{x} and is therefore positive definite. Therefore, SBE does not impose any additional constraints on the filter for the purpose of obtaining the additional input estimate.

IMPLICATIONS OF THE NECESSARY CONDITIONS

Here, we are trying to make a 'one-shot' estimate of the input vector without having the benefit of 'input-dynamics.' Therefore, the filter necessitates the availability of sufficient observations by imposing the condition ($q \leq n \leq s$).

The requirement that (HB) be of full rank indicates that all the q inputs must appear in the observations. If $\text{rank}(HB) = \rho(HB) < q$ then it would mean that all of q input components do not directly affect the observations in any way. However, they may do so through the states at subsequent stages and may be estimated later [8,9]. Therefore, ($\rho(HB) = q$) may be interpreted as the 'observability' condition for the input.

Condition (31b) is not a new one and merely requires that a reliable prior estimate must exist. It is always true in case of a properly formulated problem, as long as the system noise covariance Q is not taken to be a null matrix.

PROPERTIES OF THE ESTIMATE

If the estimate (23) is to be unbiased, it must satisfy the requirement

$$E(\hat{X}) = E(X) \quad (32)$$

$$\text{where } E(X) = E \begin{bmatrix} x^0 \\ x_{i+1} \\ u_i \end{bmatrix} = \begin{bmatrix} E(x_{i+1}^0) \\ E(u_i) \end{bmatrix} = \begin{bmatrix} E(x_{i+1}^0) \\ u_i \end{bmatrix} \quad (33)$$

Taking the expectation of Eq. (23) we get

$$E(\hat{X}) = E(\bar{X}) + \phi^{-1} H^{*T} R^{-1} E(z - H^* \bar{X}) \\ = E(\bar{X}) + \phi^{-1} H^{*T} R^{-1} H^* E(X - \bar{X}) \quad (34)$$

The last equality in (34) is obtained from Eq. (12) and from the fact that v_{i+1} is a zero mean vector. Because \bar{x} is an unbiased estimate of x :

$$E(\bar{X}) = \begin{bmatrix} E(\bar{x}) \\ 0_q \end{bmatrix} = \begin{bmatrix} E(x) \\ 0_q \end{bmatrix} \quad (35)$$

Using Eqs. (33) and (35) it is possible to write the expectation of $X - \bar{X}$ in the following form.

$$E(X - \bar{X}) = E \begin{bmatrix} x \\ u \end{bmatrix} - E \begin{bmatrix} x \\ 0_q \end{bmatrix} = \begin{bmatrix} E(x - \bar{x}) \\ u \end{bmatrix} = \begin{bmatrix} 0_n \\ u \end{bmatrix} \quad (36)$$

Due to the particular form of $E(X - \bar{X})$ in the above equation, it can be easily confirmed that the following identity is true.

$$\phi^{-1} \begin{bmatrix} M^{-1} & 0_{nq} \\ 0_{qn} & 0_{qq} \end{bmatrix} E(X - \bar{X}) = 0_{n+q} \quad (37)$$

Adding this null vector to the right side of Eq. (34), we get

$$E(\hat{X}) = E(\bar{X}) + \phi^{-1} \left\{ H^{*T} R^{-1} H^* + \begin{bmatrix} M^{-1} & 0_{nq} \\ 0_{qn} & 0_{qq} \end{bmatrix} \right\} E(X - \bar{X}) \quad (38)$$

But, the quantity in the brackets in this equation is ϕ itself, Eq. (24b). Therefore, the required property emerges immediately.

$$E(X) = E(\bar{X}) + E(X - \bar{X}) = E(X) \quad (39)$$

By drawing analogies with the Kalman filter described in Ref. [4], the following quantities can be defined:

$$\text{Gain} = K_{i+1}^* = \phi^{-1} H_{i+1}^{*T} R_{i+1}^{-1} \quad (40)$$

$$\text{Covariance} = P_{i+1}^* = \phi^{-1} = E \left\{ \begin{array}{l} (X_{i+1} - \bar{X}_{i+1}) \\ (X_{i+1} - \bar{X}_{i+1})^T \end{array} \right\} \quad (41)$$

Using Eq. (7), corresponding quantities for the n-dimensional system of interest can be deduced.

DISCUSSIONS

The Bayesian estimate derived in this part can be calculated under conditions which can easily be satisfied, (31). In fact, these conditions were assumed to be true even for obtaining the minimum variance input estimate in Ref. [1]. Therefore, the Bayesian estimate does not impose any new restrictions, and at the same time, it makes use of the 'a priori' information in the form of \bar{x}_{i+1} and H_{i+1}^* . Under certain conditions, this information was lost in the RES, [5].

No approximations were made and the Eq. (23) represents a valid and a correct Bayesian estimate. Even if Bayesian estimation is not a new technique, its application to simultaneous state and input estimation is. Also, state augmentation has been used often in the literature for estimating biases and unknown time-distributed inputs, but not for one-stage estimates. The scheme proposed here is to be employed in conjunction with a decision rule to estimate and detect any inputs, as they occur. Therefore, it is suitable for improving the performance of the RES where immediate detection of sudden changes in state (inputs) is considered equally as important as obtaining a good overall state estimate.

SBE still remains to be investigated further. The optimality or sub-optimality properties have to be determined under the orthogonality condition. The fact that SBE retains the memory of the filter, gives a strong indication that it will give a much better state estimate in the presence of inputs. Further research concerning this approach and computer simulations of the RES incorporating the SBE are necessary.

ACKNOWLEDGEMENT

This paper is submitted by Dr. R. Sonalkar to the School of Engineering, Rensselaer Polytechnic Institute, Troy in partial fulfillment of the requirements for the degree of Doctor of Philosophy.

REFERENCES

1. Sanyal, P. and Shen, C. N., "Bayes Decision Rule for Rapid Detection and Adaptive Estimation Scheme with Space Applications", IEEE Transactions, Vol. AC-19, #3, June 1974, pp 228-231.
2. Sonalkar, R. V. and Shen, C. N., "Rapid Estimation and Detection Scheme for Unknown Discretized Rectangular Inputs", IEEE Transactions, Vol. AC-20, #1, Feb. 1975, pp 142-144.
3. Willsky, A. S. and Jones, H. L., "A Generalized Likelihood Ratio Approach to State Estimation in Linear Systems Subject to Abrupt Changes", Proceedings of IEEE Conference on Decision and Control, Phoenix, Arizona, Nov. 1976, pp. 846-853.
4. Bryson, A. E. and Ho, I.C., Applied Optimal Control, Blaisdell Publishing Co., Waltham, Mass. 1969.
5. Sanyal, P. and Shen, C. N. "Bayes Decision Rule for Rapid Detection and Adaptive Estimation Scheme with Space Applications", Proceedings of the Joint Automatic Control Conference, Columbus, Ohio, June 1974.
6. Sonalkar, R. V. and Shen, C. N., "Rapid Estimation and Detection Scheme for Unknown Discretized Rectangular Inputs", Proceedings of the Joint Automatic Control Conference, Austin, Texas, June 1975.
7. Sage, A. P. and Melsa, J. L., Estimation Theory with Applications to Communications and Control, McGraw-Hill Book Co., New York 1971.
8. Sonalkar, R. V. and Shen, C. N., "Ways Obstacle Detection by Rapid Estimation Scheme from Noisy Laser Rangefinder Readings", Proceedings of the Milwaukee Symposium on Automatic Computation and Control, Milwaukee, Wisconsin, April 1975, pp 291-296.
9. Sonalkar, R. V., "A Decision Directed Rapid Estimation of States for System Subject to Unknown Input Sequences", Ph.D. Dissertation, Rensselaer Polytechnic Institute, Troy, N.Y., Dec. 1975.

ORIGINAL PAGE IS
OF POOR QUALITY

Task A.3 Estimation of Laser Rangefinder Errors - T. Ostroski
Faculty Advisor: Prof. C. N. Shen

The detection of discrete obstacles using laser rangefinder data involves the mathematical processing of range data contaminated by instrument measurement noise. The instrument noise should be determined in advance of specifying parameters to be used in evaluating a system for enhancing the images of potential obstacles. In the past the mean and variance of the noise were assumed and employed in computer simulations of the edge enhancement procedures. The actual determination of the statistics of the noise for an actual instrument was not attempted.

The purpose of this task was to establish the actual noise statistics of an existing laser rangefinder. Methods for determining the noise were developed and applied to a set of such data provided by Mr. Dobrotin of the Jet Propulsion Laboratory. Details of the procedure and the results are provided in the reprint of the paper which follows.

PRESENTED AT THE SEVENTH ANNUAL MODELING AND SIMULATION CONFERENCE, PITTSBURGH, PA., April 1976 and published in the Proceedings of the Conference.

ACCURACY ESTIMATE OF THE LASER RANGEFINDER FOR MARS ROVER*

T. Ostroski and C. N. Shen
Rensselaer Polytechnic Institute
Troy, New York
12181

ORIGINAL PAGE IS
OF POOR QUALITY

ABSTRACT

A method was developed to determine the accuracy of a rangefinder when errors exist due to the test setup. An analytic procedure was developed to evaluate actual data from a test performed on the laser rangefinder for the Mars rover project.

INTRODUCTION

The laser rangefinder and a television camera are two alternatives being considered to supply the data for the terrain modeling, obstacle detection, and path selection systems for the Mars autonomous rover. The advantage of the laser rangefinder is that actual distance to obstacles can be found. Therefore, it is important to know the accuracy of the rangefinder. The actual data, which is used in this paper, was taken from a test on a prototype rangefinder constructed at the Jet Propulsion Lab as part of the Mars Rover Project.

STATEMENT OF THE PROBLEM

The problem is to estimate the accuracy of a rangefinder given the data from an actual test run. The field of scan for this test is a flat plane with no obstacles. If obstacles exist they must be removed from the range data set. The inaccuracies involved in the test scan come from many sources of error. These sources of error are in the device itself and possibly in the test setup also. Any errors due to the test setup must be eliminated in the estimate of the error for the device itself.

THE RANGE DATA MATRIX

A diagram of the scanning device relative to the scanned area is shown in Figure 1. Point A is the scanning device itself. Point B is the point on the line, AB, which intersects the horizontal plane that includes the scanned area. Line AB is perpendicular to this plane. Z_0 is the distance from A to B.

Although a rectangular coordinate system is given, the scanning scheme is in a spherical coordinate system. In figure 1, the elevation angle, θ , and the azimuthal angle, ϕ , are divided into steps. The size of the steps are $\Delta\theta$ and $\Delta\phi$ for the elevation step and azimuthal step, respectively. The

actual position of the rectangular coordinate system is arbitrary (the coordinate system has ϕ_{\min} equal to 0° from the y axis for convenience).

The data matrix, R_{ij} , is an $m \times n$ matrix, where m is the number of elevation steps and n is the number of azimuthal steps. The quantity, R_{ij} , corresponds to the i th elevation angle step and the j th azimuthal angle step. Therefore, R_{i1} corresponds to θ_{\min} and ϕ_{\min} and R_{mn} corresponds to θ_{\max} and ϕ_{\max} .

METHOD OF ANALYSIS

Two approaches are given in this section. The choice of the method depends upon how well the test setup has been calibrated.

1. Two-Dimensional Accuracy Analysis - For an ideal test setup, all range data values for a given elevation angle should be equal. That is, if the axis of the rangefinder is perpendicular to the horizontal plane, varying the azimuth angle with a constant elevation angle will sweep an arc of a circle on the horizontal surface with the center at point B.

Under this condition, the data for all azimuthal angle steps at a given elevation angle can be averaged for each of m elevation steps. These m averaged values are called \bar{R}_i and are computed by the following equation:

$$\bar{R}_i = \frac{1}{n_i} \sum_{j=1}^{n_i} R_{ij} \quad (1a)$$

where n_i is the number of range data points in row i .

The \bar{R}_i can be plotted to create a two dimensional profile of the range data. This plot is useful for a visual inspection of the linearity of the elevation mechanism. The standard deviation, S_i , can then be calculated for the data points in each row, i , using the \bar{R}_i , in the formula:

$$S_i = \sqrt{\frac{\sum_{j=1}^{n_i} (R_{ij} - \bar{R}_i)^2}{n_i - 1}} \quad (1b)$$

A least-squares fit to the two-dimensional plot is valuable for this problem. It can provide a better

analysis of the non-linearity than a visual inspection. Also, values of Z_0 and θ_{\min} , which are shown in Figure 1, can be calculated from the fitted line and compared to the values measured for the test.

In the least-squares fit, the estimated equation is of the form:

$$v = au + b \quad (2)$$

To facilitate the estimate, another coordinate system was used. This transformation is shown in Figure 2. In the u v coordinate system, the rangefinder (point A) is the origin; and, to eliminate θ_{\min} from the analysis, the mean value for the first elevation angle value is placed on the u axis.

The values of u_i and v_i can be obtained from the mean values, \bar{R}_i , of the rows of R_{ij} by the following equations, where $\Delta\theta$ is the elevation step size:

$$u_i = \bar{R}_i \cos[(i-1)\Delta\theta] \quad (3a)$$

$$v_i = \bar{R}_i \sin[(i-1)\Delta\theta] \quad (3b)$$

The equations used to calculate the values of a and b in equation (2) can be obtained from a probability [1] or computing methods text under the headings, "linear regression". They are as follows:

$$b = \frac{\sum_{i=1}^m u_i v_i - (\sum_{i=1}^m u_i)(\sum_{i=1}^m v_i)}{n \sum_{i=1}^m (u_i)^2 - (\sum_{i=1}^m u_i)^2} \quad (4)$$

$$a = \frac{1}{m} \sum_{i=1}^m v_i - \frac{b}{m} \sum_{i=1}^m u_i \quad (5)$$

The estimated value of Z_0 is computed using the fact that slope of the line in Figure 2, \overline{AB} , is the negative of the reciprocal of the slope, a , of the estimated line. The equation for the line \overline{AB} is

$$v = -\frac{1}{a} u \quad (6)$$

Solving equations (2) and (6) simultaneously, the coordinates of point B, u_0 and v_0 , are obtained:

$$u_0 = -\frac{ab}{1+a^2} \quad (7)$$

$$v_0 = \frac{b}{1+a^2} \quad (8)$$

The length of Z_0 can then be calculated by taking the square root of the sum of the squares of u_0 and v_0 from equations (7) and (8):

$$Z_0 = \sqrt{\left(-\frac{ab}{1+a^2}\right)^2 + \left(\frac{b}{1+a^2}\right)^2} \quad (9)$$

The θ_{\min} can be calculated using the value of Z_0 and b . The angle between the v axis and \overline{AB} in Figure 2 is equal to θ_{\min} . Therefore, θ_{\min} can be calculated as follows:

$$\theta_{\min} = \arccos \frac{Z_0}{b} \quad (10)$$

The differences, e_i , between the actual \bar{R}_i values and the estimated line shown in Figure 3 are very useful for analysis. To calculate, e_i , the equation of the line \bar{R}_i that passes through the origin is determined. The equation for it is:

$$v = u [\tan \Delta\theta(i-1)] \quad (11)$$

If equations (2) and (11) are solved simultaneously for u , the value is called u'_i and is given in the following equation:

$$u'_i = \frac{b}{\tan[\Delta\theta(i-1)] - a} \quad (12)$$

and then the horizontal projection of the error, $(e_u)_i$, is:

$$(e_u)_i = u_i - u'_i \quad (13)$$

Finally, the errors, e_i , between the \bar{R}_i and the fitted line, are calculated by dividing $(e_u)_i$ by the cosine of $(i-1)\Delta\theta$:

$$e_i = \left(u_i - \frac{b}{\tan[\Delta\theta(i-1)] - a} \right) / \cos[\Delta\theta(i-1)] \quad (14)$$

2. Three Dimensional Accuracy Analysis - The three-dimensional accuracy analysis is desired when there is a "tilt" in the test setup. In the two dimensional analysis, any such "tilt" will show up as an apparent increase in the error for each row.

The methods in this section also compute the "tilt" so that the rangefinder can be aligned to be perpendicular to the horizontal plane. A visual inspection of the range data points can reveal whether or not there is a "tilt". General trends of increasing or decreasing values of R_{ij} , as j goes from 1 to n , indicate that a "tilt" exists.

The range data is given in a polar coordinate system so the data must first be transformed into the x , y , z coordinate system shown in Figure 1. The conversion formulae are:

$$x_{ij} = R_{ij}(\cos \theta_i) \cos \phi_j \quad (15)$$

$$y_{ij} = R_{ij}(\cos \theta_i) \sin \phi_j \quad (16)$$

$$z_{ij} = R_{ij}(\sin \theta_i) \quad (17)$$

where

$$\theta_i = \theta_{\min} + (i-1)\Delta\theta \quad (18)$$

$$\phi_j = (j-1)\Delta\theta \quad (19)$$

The plane which contains the range data points can also be estimated by a least-squares estimate. The equation of the plane will be:

$$z = w_1 x + w_2 y + w_3 \quad (20)$$

The objective function that must be minimized is:

$$J = \sum_{i=1}^m \sum_{j=1}^n [z_{ij} - (w_1 x_{ij} + w_2 y_{ij} + w_3)]^2 \quad (21)$$

Taking partial derivatives with respect to the coefficients, w_1 , w_2 , w_3 , and setting them equal to zero:

we obtain;

$$W = Q^{-1}P \quad (22)$$

The matrices are defined as:

$$Q = \begin{bmatrix} \sum \sum x_{ij}^2 & \sum \sum x_{ij} y_{ij} & \sum \sum x_{ij} z_{ij} \\ \sum \sum x_{ij} y_{ij} & \sum \sum y_{ij}^2 & \sum \sum y_{ij} z_{ij} \\ \sum \sum x_{ij} z_{ij} & \sum \sum y_{ij} z_{ij} & \sum \sum z_{ij}^2 \end{bmatrix} \quad (23)$$

$$P = \begin{bmatrix} \sum \sum x_{ij} z_{ij} \\ \sum \sum y_{ij} z_{ij} \\ \sum \sum z_{ij}^2 \end{bmatrix} \quad (24)$$

$$\underline{v} = \begin{bmatrix} v_1 \\ v_2 \\ v_3 \end{bmatrix} \quad \text{and } \Sigma \Sigma \text{ is } \begin{matrix} m & n \\ \Sigma & \Sigma \\ i=1 & j=1 \end{matrix} \quad (25)$$

These equations can be solved using a matrix solution routine to find the coefficient vector \underline{v} , if Q is nonsingular.

The actual range data can be compared to the estimated plane by generating the values of range data that correspond to the estimated plane. These range values are called \hat{R}_{ij} . The equation for \hat{R}_{ij} is derived by substituting equations (15), (16) and (17) into equation (20) and solving for R_{ij} :

$$\hat{R}_{ij} = \frac{w_3}{\sin \theta_1 - \cos \theta_1 (w_1 \cos \phi_j + w_2 \sin \phi_j)} \quad (26)$$

where θ_1 and ϕ_j are given in equations (18) and (19). This primed range data matrix, \hat{R}_{ij} , can be subtracted from the original range data matrix, R_{ij} , to form an error matrix, R_{ij}^* :

$$R_{ij}^* = R_{ij} - \hat{R}_{ij} \quad (27)$$

The R_{ij}^* matrix shows the difference between the estimated plane and the original data.

Using equations (26) and (27) the matrices, \hat{R}_{ij} and R_{ij}^* , values were calculated. The R_{ij}^* values were manipulated to provide more useful data. First, the values were averaged in each row and called r_i^* :

$$r_i^* = \frac{1}{n_i} \sum_{j=1}^{n_i} R_{ij}^* \quad (28)$$

where n_i is the number of data points in row i .

Next, the standard deviation of the values in each row, s_i^* , were calculated using the following equation:

$$s_i^* = \sqrt{\frac{\sum_{j=1}^{n_i} R_{ij}^{*2}}{n_i - 1}} \quad (29)$$

The values for r_i^* and s_i^* are shown in Table 1. The means and standard deviations, calculated in the three-dimensional analysis, correspond to \bar{R}_i and S_i , calculated in the two-dimensional analysis. The starred values, however, are computed taking the "tilt" into consideration.

The direction of the "tilt", as projected on the x, y axes, is needed to align the rangefinder. This direction, \underline{d} , shown in Fig. 1, can be computed by taking the gradient of Equa. (20). The vector \underline{d} is given by

$$\underline{d} = [w_1 \ w_2]^T \quad (30)$$

If no tilt exists, \underline{d} will be a zero vector.

THE MARS ROVER: AN APPLICATION

The techniques shown in this paper were developed to analyze actual test data from the laser rangefinder developed for the Mars Rover from tests performed at Jet Propulsion Lab., Pasadena, CA, and obtained from Mr. B. Dobrotin.

The rangefinder, consisting of a laser photodetector, and an electronic circuit, measures time of flight by a time-to-pulse-height conversion technique. It uses a 10 bit A/D converter to obtain

a digital output signal. Six values are measured for each position; the final five are averaged to get the range value for that position. The beam orientation is changed by moving a mirror that positions the laser beam with two stepping motors. For the test data, there were 30 elevation steps and 50 azimuthal steps. The range data set for the laser rangefinder is shown in Fig. 3. The range points that fell on an obstacle were set equal to zero so the computer programs for the analysis would skip these points.

The parameters for the test setup [2] for this data are: $Z_0 = 636.0 \text{ mm}$, $\Delta\theta = .3307 \text{ degrees/step}$, $\Delta\phi = .3059 \text{ degrees/step}$, $\theta_{\min} = 35.04 \text{ degrees}$.

The Results - The values of the mean, \bar{R}_i , and standard deviation, S_i , computed from equations (1a) and (1b) and number of data points for each row of the range data are shown in Table 1. Using these mean values, \bar{R}_i , and equations (2) thru (5), the least-squares estimate of the line passing through these points was made:

$$v = .62859 \quad u = 792.95 \quad (31)$$

The estimated value of Z_0 , using Equa. (9), is 671.3 mm. From Equa. (10), the estimated value of θ_{\min} is calculated to be 32.15° .

The values of e_i in Table 1 show the difference between the \bar{R}_i and the estimated line in Equa. (2) as shown in Fig. 2. These values were calculated using Equa. (14). Any trends in the \bar{R}_i values can be observed in the changes of the values of e_i .

This analysis was given only as an illustration. There is a "tilt" in this range data, so the standard deviations, S_i , are not good estimates of the performance of the laser rangefinder.

The "tilt" in the data can be observed in Fig. 2 by comparing the left- and right-most columns of the range data. In 22 of the 30 rows, the first element is smaller than the last; and in the other rows, they are equal. This indicates that "tilt" probably exists and that the three-dimensional analysis should be applied.

For the least-square estimate of the plane of the data, the matrix equations, (22) thru (25) were solved for the vector, \underline{v} . Equation (20) for this estimate is:

$$z = .03946 x + .03383 y + 678.0 \quad (32)$$

The direction of the tilt, \underline{d} , was calculated to be $[\ .03946 \ .03383]^T$ using Equa. (28). In the top view of Fig. 1, the position of \underline{d} is shown relative to the plane of the scan in the x, y plane. This direction of the "tilt" is in agreement with the earlier observations of the range data.

INTERPRETATION OF THE RESULTS

A comparison of these statistical results of values provides useful information. Both the e_i and the r_i^* shown in Table 1 indicate a trend of curvature in the data. Because it appears in the three-dimensional analysis, the trend is not due to the tilt of the plane. This non linearity is from the device itself and originates either in the elevation mechanism, the range measurement apparatus, or both.

ORIGINAL PAGE IS OF POOR QUALITY

The standard deviations of the three-dimensional analysis are in general smaller than those of the two-dimensional analysis. This is expected because the three dimensional analysis removes the added errors due to the tilt in the test. The standard deviations, S_i^* , range from approximately 2 to 7 mm. Studying these S_i^* , one will notice a trend of increasing error as the distance of the range value increases (Row 1 has the largest range values). Because the change is not significant, however, an actual value of the error cannot be established. The standard deviations S_6^* and S_{30}^* are 7.74 mm and 5.12 mm. They are larger by about 4 mm than the other values of S_i^* around them. In subsequent tests, the standard deviations of these rows should be checked to see if this problem re-occurs.

Before the data in Table 1 is interpreted further, the quantization error must be estimated. The standard deviation, S_q , of the quantization error can be found independently of the scan by the following formula, where Δ is the difference between successive quantization levels:

$$S_q = \sqrt{\frac{\Delta^2}{12}} \quad (33)$$

For this data set, Δ equals 9mm; therefore, S_q equals 2.6 mm. Except for rows 6 and 30, the S_i^* range from 2.9 to 4.7 mm. Most of the inaccuracy therefore is due to quantization error. The next largest source of error is the nonlinearity of the range readings. The inaccuracy due to this nonlinearity makes the performance of the rangefinder poor for the range of approximately 1 to 1.3 meters. Modifications to the rangefinder should be made if it is to be used in this range.

CONCLUSION

This paper has presented two methods to analyze the accuracy of a rangefinding device.

The two-dimensional analysis is useful when the rangefinding device has been aligned so that its vertical axis is perpendicular to the scanned plane. The errors, e_i , introduced from the rangefinding device or other sources can be observed in Table 1 of the means \bar{R}_i , and standard deviations, S_i . A visual inspection of the e_i will reveal any nonlinearities of the data. These nonlinearities of the system are shown at different elevation angles and, hence, at different range distances.

The three-dimensional analysis is used when a "tilt" exists between the scanned plane and the vertical axis of the rangefinding device. In this method, the plane of the scan is determined using a least-squares estimate. From the equation of the estimated plane, the vertical axis can be realigned, for the actual device and the test can be run again. Also, values of range data can be computed from the equation of the estimated plane. The difference of these values and the actual range data can be used to give a rough estimate of the accuracy when "tilt" exists.

If it is possible to make multiple tests of the rangefinder, the best approach is to first correct the alignment of the rangefinder using the second method, and then use the first method to analyze the data from the rangefinder test.

The methods just described show the errors of the rangefinding device as the elevation angle, θ , changes or, equivalently, as the distance of the measurement increases. The source of these errors are the elevation angle positioning mechanism or the distance measuring device itself. Other sources of error that are included in the error estimate are quantization error and error due to noise in the environment. The quantization error can be estimated independently and compared to the final results.

The change of range reading with the intensity of the reflected pulse is also important [3]. The intensity of the reflected pulse can be changed by changing the reflecting surface or by changing the angle of the reflecting surface with the incident beam. The errors due to the latter are measured by the methods in this paper; because as the distance of a range data increases, the angle that the surface forms with the beam also increases [4]. However, these errors and the errors due to increasing distance of the measurement cannot be separated in the analysis. It is recommended that a testing scheme be constructed that could measure the errors due to changes of intensity.

Table 1. Statistical Results

Row	\bar{R}_i	S_i	e_i	r_i^*	S_i^*	n_i
i	mm	mm	mm	mm	mm	data/row
1	1264.00	5.71	2.23	2.73	4.45	24
2	1252.52	5.14	2.23	2.35	3.69	23
3	1239.96	5.87	0.90	1.43	3.81	25
4	1230.58	4.56	2.50	3.05	4.34	26
5	1218.97	4.27	1.65	2.72	4.30	29
6	1210.18	5.65	3.39	4.90	7.74	33
7	1196.57	2.63	0.09	1.93	4.65	37
8	1187.27	4.17	0.88	2.55	4.66	37
9	1177.19	3.93	0.69	2.18	3.74	37
10	1166.54	4.78	-0.27	1.05	4.33	37
11	1154.62	5.12	-2.71	-1.65	3.51	50
12	1145.52	4.85	-2.51	-1.61	3.39	50
13	1135.46	5.44	-3.46	-2.71	4.14	50
14	1127.28	4.99	-2.71	-2.11	3.33	50
15	1118.58	5.17	-2.65	-2.20	3.27	50
16	1110.62	4.58	-2.03	-1.71	3.23	50
17	1101.02	5.81	-3.21	-3.03	4.14	50
18	1093.48	5.17	-2.50	-2.45	4.01	50
19	1085.44	4.79	-2.44	-2.52	3.93	50
20	1078.72	3.79	-1.22	-1.42	3.36	50
21	1070.44	4.44	-1.71	-2.03	3.84	50
22	1063.80	3.77	-0.71	-1.14	3.17	50
23	1055.94	3.32	-1.06	-1.61	3.40	50
24	1040.96	4.52	0.32	-0.34	3.30	50
25	1043.60	3.90	1.18	0.42	2.88	50
26	1036.86	4.46	1.53	0.66	3.44	50
27	1029.24	3.36	0.87	-0.10	3.31	50
28	1023.72	4.43	2.19	1.12	3.02	50
29	1017.80	4.99	2.98	1.81	3.40	50
30	1013.80	6.15	5.57	4.31	5.12	50

REFERENCES

- Walpole, R. & Myers, R., Probability and Statistics for Engineers, MacMillan Co., New York, 1972, pp 281-284.

*Research sponsored by NASA Grant NSG-7184

- 2. Smith, T.L., "Test Setup for Laser Area Scan and Mag Tape- Sept. 15, 1975", unpublished, Jet Propulsion Lab., Pasadena, CA.
- 3. Smith, T.L., "AI Laser Rangefinder Performance" August 25, 1975, unpublished, Jet Propulsion

Lab., Pasadena, California.

- 4. Friedman, M. & Shen, C.N., "The Effect of Laser Measurement Reflection Error on Range Data Processing", Milwaukee Symposium on Automatic Computation and Control, Milwaukee, Wisc. Apr. '75.

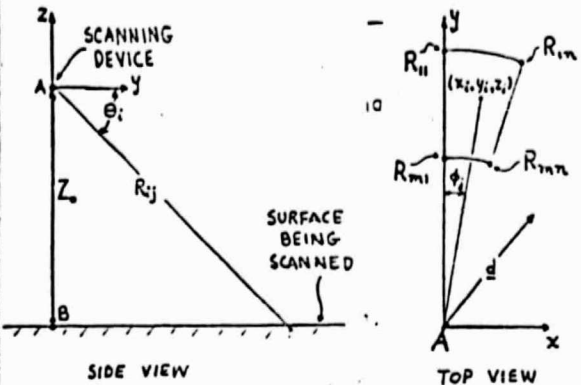


Figure 1-Diagram of the test setup

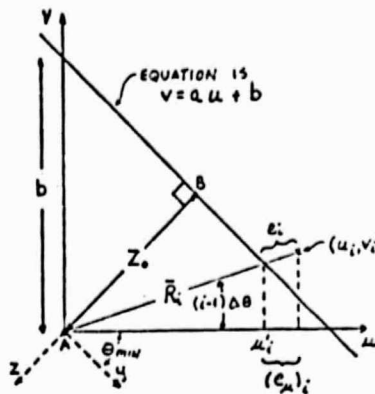


Figure 2 - The u,v Coordinate System

ROW	COLUMN	30	40	50
1	1	0	0	0
10	1	1155	1155	1155
20	1	1071	1071	1071
30	1	1013	1013	1013
1	2	0	0	0
10	2	1147	1147	1147
20	2	1063	1063	1063
30	2	1005	1005	1005
1	3	0	0	0
10	3	1130	1130	1130
20	3	1046	1046	1046
30	3	988	988	988
1	4	0	0	0
10	4	1113	1113	1113
20	4	1029	1029	1029
30	4	971	971	971
1	5	0	0	0
10	5	1096	1096	1096
20	5	1012	1012	1012
30	5	954	954	954
1	6	0	0	0
10	6	1079	1079	1079
20	6	995	995	995
30	6	937	937	937
1	7	0	0	0
10	7	1062	1062	1062
20	7	978	978	978
30	7	920	920	920
1	8	0	0	0
10	8	1045	1045	1045
20	8	961	961	961
30	8	903	903	903
1	9	0	0	0
10	9	1028	1028	1028
20	9	944	944	944
30	9	886	886	886
1	10	0	0	0
10	10	1011	1011	1011
20	10	927	927	927
30	10	869	869	869
1	11	0	0	0
10	11	994	994	994
20	11	910	910	910
30	11	852	852	852
1	12	0	0	0
10	12	977	977	977
20	12	893	893	893
30	12	835	835	835
1	13	0	0	0
10	13	960	960	960
20	13	876	876	876
30	13	818	818	818
1	14	0	0	0
10	14	943	943	943
20	14	859	859	859
30	14	801	801	801
1	15	0	0	0
10	15	926	926	926
20	15	842	842	842
30	15	784	784	784
1	16	0	0	0
10	16	909	909	909
20	16	825	825	825
30	16	767	767	767
1	17	0	0	0
10	17	892	892	892
20	17	808	808	808
30	17	750	750	750
1	18	0	0	0
10	18	875	875	875
20	18	791	791	791
30	18	733	733	733
1	19	0	0	0
10	19	858	858	858
20	19	774	774	774
30	19	716	716	716
1	20	0	0	0
10	20	841	841	841
20	20	757	757	757
30	20	699	699	699
1	21	0	0	0
10	21	824	824	824
20	21	740	740	740
30	21	682	682	682
1	22	0	0	0
10	22	807	807	807
20	22	723	723	723
30	22	665	665	665
1	23	0	0	0
10	23	790	790	790
20	23	706	706	706
30	23	648	648	648
1	24	0	0	0
10	24	773	773	773
20	24	689	689	689
30	24	631	631	631
1	25	0	0	0
10	25	756	756	756
20	25	672	672	672
30	25	614	614	614
1	26	0	0	0
10	26	739	739	739
20	26	655	655	655
30	26	597	597	597
1	27	0	0	0
10	27	722	722	722
20	27	638	638	638
30	27	580	580	580
1	28	0	0	0
10	28	705	705	705
20	28	621	621	621
30	28	563	563	563
1	29	0	0	0
10	29	688	688	688
20	29	604	604	604
30	29	546	546	546
1	30	0	0	0
10	30	671	671	671
20	30	587	587	587
30	30	529	529	529

Figure 3 - The Range Data Matrix of R_{ij}

ORIGINAL PAGE IS
OF POOR QUALITY

Task B. Path Selection System Simulation - B. Longendorfer
Faculty Advisor: Prof. D. K. Frederick

The overall objective of this task is to define a path selection system for the exploration of the surface of a planet using Mars as a case. Because of the delay introduced by one-way communication to Earth from Mars (on the order of twenty minutes), the vehicle must be able to sense its environment and direct its own movements without human assistance. Accordingly, algorithms are sought which will organize the collected data into an appropriate "world model", and utilize it in choosing an optimal safe path.

The particular methods investigated are edge-detection techniques. Edge detection techniques require a matrix of range/pointing angle data. Sudden changes in magnitude between adjacent elements, or differences in the rate of change of these magnitudes signal the existence of "edges".

The application of these techniques to the Mars Rover requires much supporting simulation work. For example, the matrix of input data consists of laser range readings from a specified field of view, requiring the simulation of a range-finding sensor.

Practical problems arise when considering the multitude of situations that occur in the physical world. Flat field, single obstacle encounters (with which most of the theoretical work has been done) are rare. Problems such as what initialization procedures shall be used, which side of an edge (or both) constitutes an obstacle, what threshold values yield the "best" performance, etc. must be considered. At times, additional processing might be required to obtain a more complete picture.

The vehicle then must relate the resulting matrix of edges to the actual environment, through a Terrain Modeller. The Terrain Model must calculate the actual location of the obstacles sensed, their approximate size and height, their relationship to the surrounding terrain, and the location of scanned (known) and unscanned (unknown) regions. Work on the Terrain Model has reached the debugging and concept testing stage.

Once information about its surroundings is available to the vehicle, it must select a safe optimal path to its target. The method employed is called a path selection algorithm. The algorithm is necessarily influenced by the data-acquisition method in such factors as the conservatism of the method (because of the susceptibility to noise or the lack of it), and the type of obstacles which the sensor is intended to detect (discrete obstacles, slopes, positive or negative obstacles). Work on the path selection algorithm is in the planning stage.

Sensor

A laser rangefinder sensor was specified for a nominal range of three to thirty meters. Previous sensor simulations were not suited to this particular task. They allowed for only a small number of elevation angles (one to four), and these were constrained to certain values (for example, only horizontal). Azimuth

angles were similarly constrained. Clearly, the sensor used in edge detection needed to be able to generate a large matrix of readings at one time, at any angle coordinates. The sensor now programmed overcomes these defects, as well as providing for time lapse while scanning. Noise affecting the range readings is taken into account in two ways:

- (1) noise of specified type, mean, variance, maximum amplitude, natural frequency, and damping constant may be added directly to the range readings, and
- (2) the specified accuracy of the sensor may be changed by the user.

Plans for further work on the sensor include the modification of the added noise by a factor proportional to the range squared, in order to better simulate errors in time of flight measurement.

The sensor simulation uses the following method to compute range readings. It first calculates the position of the laser and the position of the location where the laser would intersect ground, both with respect to the vehicle, assuming no slopes. It transforms both points to the planet reference frame, by its knowledge of vehicle heading, and actual in-path and cross-path slopes. It calculates the direction cosines of the line connecting the two points and steps along this beam with a user-specified increment (BEMSTP, usually set to five centimeters), until it finds itself below the actual terrain level. It enters a bisection scheme until the desired accuracy is reached. The accuracy is a user-specified input (SIMSTP) and is defined as the difference between exact measurement and the computed measurement (not as the difference between the height of the computed measurement and the terrain at that point, as in previous sensors). Efficiency of the sensor is vastly improved by the use of an initial guess at the range reading, and logic which will not recalculate transformations unless the vehicle has moved from its previous position. The initial guess is taken to be zero for the elevation angle nearest the vehicle. For other elevation angles, the guess is set equal to a value somewhat smaller than that for the elevation angle nearest to it but closer to the vehicle.

Testing of the sensor is now complete.

Scan Generator

The scan generator serves as a preprocessor for input and output for the sensor. It allows input in a variety of convenient forms and calculates the necessary azimuth and elevation angles to cover the specified field of view while maintaining a certain data density. Because of the requirement that the Kalman filter must receive only angles spaced by a constant number of degrees, the data density (number of points per square meter) will vary, sometimes quite drastically.

Input may appear in the form of a list of angles, or maximum, minimum and incremental angles, or in the form of field dimensions

such as length, width, center and maximum point spacing.

Testing is now complete.

Edge Detection Techniques

The edge detection programs had to be interfaced with the existing simulation package.

The edge detection routines employ a Kalman filter, which is performed separately on each row and each column. Row processing looks for changes in the magnitude of range readings (vertical edges), while column processing looks for both magnitude and slope changes (horizontal edges). The Kalman filter predicts values for each element of the array in succession, and computes the probability of an edge having occurred at that stage based on factors such as the difference between actual and expected values, the probability that an edge will occur, the cost of making a wrong decision on the location of the edge, etc. Bayes' Risk calculations weighted by these considerations make the actual decision.

The performance of the edge detection routines has been tested by generating a terrain with the simulation package, measuring ranges with the sensor, and attempting to reconstruct the edges with the computer programs. Varying success has been attained, as shown in Figures 1 through 5. Problems identified here will be explored further in months to come.

The bottom edges of boulders and the far edges of craters have not been shown by the program. To remedy the situation, two courses are presently being pursued. One possible solution is to replace some of the threshold values (originally programmed as constants) with variables, and re-test the performance. Another solution is to install an auxiliary test to look specifically for an important situation not now being identified. A "moving average" or constantly updated average value, will flag changes in slope greater than this average plus a tolerance or expected changes that fail to occur (i.e. changes less than this average minus a tolerance). The first case would signal the far edge of a negative obstacle while the second case is that of the near edge of a positive obstacle. At present, the "moving average" is able to be engaged or disengaged by a flag so that its effect may be studied. The tolerance itself is selected as a fraction of the computed average difference or as the value computed assuming the maximum transversible slope.

Noise seems to have very little effect on the performance of the Kalman filter. Figures 4 and 5 show the effects of unfiltered white noise, which was added independently to each of the range readings. Range readings differ by as much as twenty centimeters along the same row (which should ideally have exactly the same readings, since they result from identical elevation angles).

Another problem is the correct initialization procedure to follow. Until recently, initialization involved calculating expected range readings and changes in range readings given that the surrounding terrain was a flat plane. Changes in slopes between elements of a column were done the same way. However, a new initialization procedure is being tried at present. Rows and columns are initiated to the range reading actually obtained. If an edge is actually present there, it will occur at the next stage instead. The small inherent error will be more than compensated for by the lack of initialization error on slopes, which could possibly block off an entire forward path.

Terrain Model

The Terrain Model interprets the data obtained from the sensor and edge detection routines, and translates it into an organized, easily understandable form. The Path Selection Algorithm is then freed from the concern for which method was actually used to obtain the data, and it can be a much more generally applicable program.

The Terrain Model presently being developed divides the general region of the vehicle and target into a grid of squares, and uses them as a type of obstacle map to provide memory.

There are several stages preceding the construction of the final obstacle map. First, the edge matrix provided by the edge detection routines must be scanned for edges. The model must decide on which side of the edge (or both) the obstacle lies, and whether the obstacle is positive or negative. This is currently determined by taking an average range over the proposed obstacle (i.e. that terrain which is between one edge and another, where an edge is defined as the beginning or end of a row or column or as the edge identified by the detection programs). The average range is compared to a value plus or minus a threshold. The comparison value currently corresponds to that for flat ground, but a better comparison of the known surface area (such as prediction from orthogonal polynomial least squares) will soon be employed. This is an example of the interaction of the terrain model and the edge detection routines. Second, all matrix elements determined to be within the obstacle are marked according to type and blocked out. Third, all squares on the obstacle map of the environment which contain any part of the region scanned by an edge in the edge matrix are also marked with the obstacle type. This can be achieved by using attitude data and some geometry to obtain the planet (x,y,z) coordinates at the scan point. Projecting the obstacle location on to the xy-plane yields the map location. Actually, this is done at any point of the entire region sampled by one data point which will cause a new square to be blocked on the obstacle map. Further information may be obtained and included in the map such as a height code, which would be useful for computing and storing slope, and flagging hazardous terrain. However, this has not as yet been incorporated in the model. Edge detection is designed to handle discrete obstacles, so that has been the main area of concentration of effort so far.

All terrain is initially labelled as unknown and is changed to another code only after it has been scanned at least once.

Certain problems remain to be dealt with. Storage and memory capabilities directly conflict in the choice of the size of the blocks on the obstacle map. However, if only a certain amount of memory is needed while a large amount of terrain is to be covered, a "rolling pointer" might be used, which would indicate the current farthest sensor reach, while old data would be overlaid with new data from a different region. Another problem is the conflicting declarations of obstacles. Depending on the conservatism of the algorithm, differences in successive measurements would make the algorithm more or less sensitive to noise.

Other assumptions include:

- (1) The vehicle has been supplied with a map of its surroundings up to a certain radius at the beginning of the simulation (otherwise a fixed sensor could never scan the field).
- (2) The sensor cannot change, add or delete angles from its scan once they are initialized.
- (3) Primary effort should be given to the detection of discrete obstacles.

Path Selection Algorithm

The problem of selecting a path given an obstacle map consisting of squares has been dealt with by C.Y. Lee, Reference 1 and F. Lallman, Reference 2.

The algorithm consists of:

- (1) identifying the known (scanned) region
- (2) finding a minimal length path to the target
- (3) following the portion of this path of maximum length until the target is reached or another scan is necessary.

The minimal length path is identified by placing numbers in ascending order in blocks adjacent to the target, adjacent to the block adjacent to the target. As long as the vehicle progresses from one number to the next lower number, it is following a minimal length path.

Problems not considered in the literature that are faced here are:

- (1) The vehicle may be more than one square in dimension of length or width.

- (2) The vehicle has inherent dynamical characteristics and cannot turn abruptly.
- (3) The vehicle scans only a small portion of its surroundings.
- (4) The vehicle cannot proceed within a certain radius of unknown terrain without losing the ability to sense obstacles that may be present.

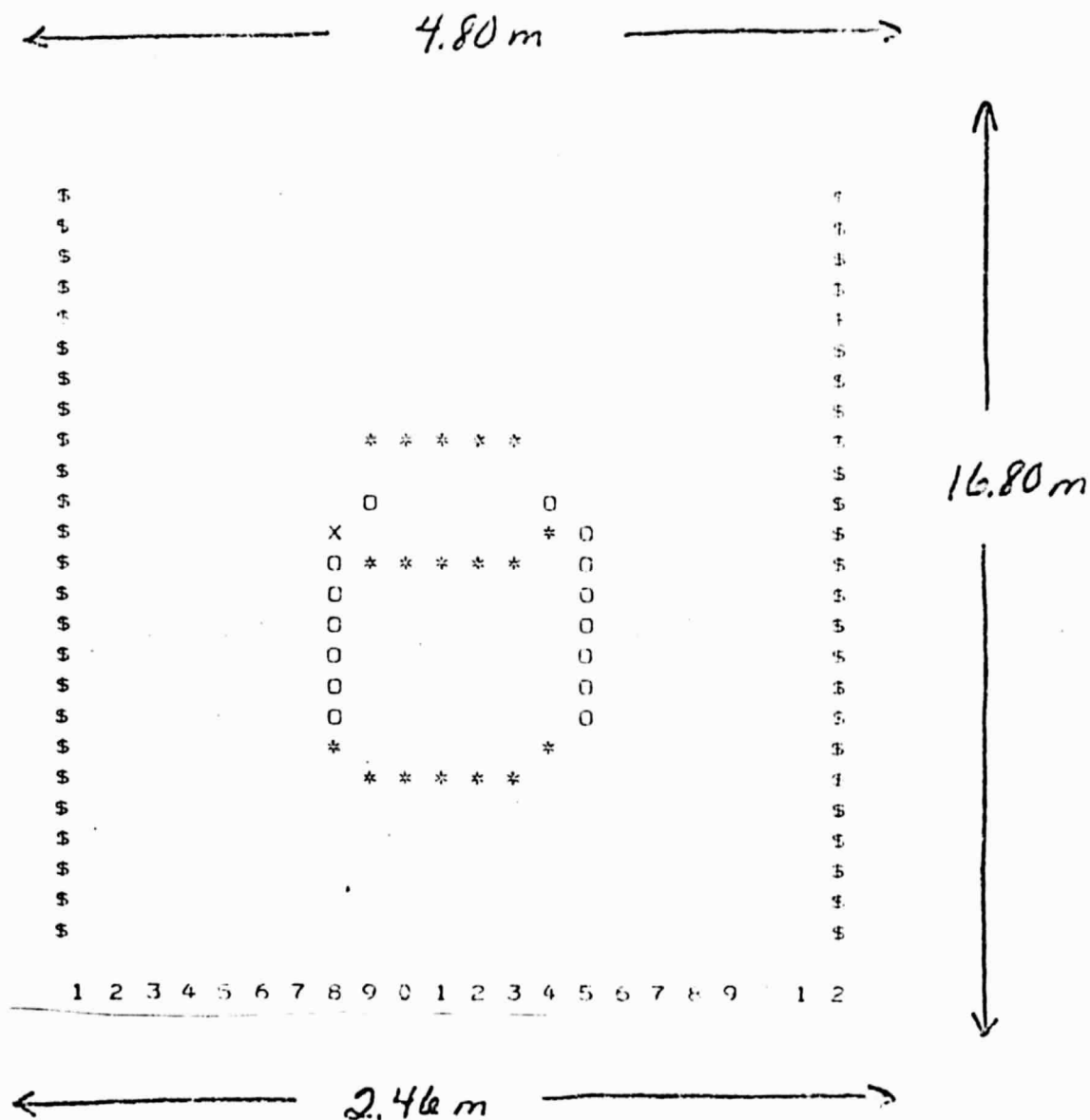
Edge detection appears to be able to overcome two of the basic problems other path selection algorithms could not easily deal with: noise, and confusion of slopes with discrete obstacles. The trade-off seems to be memory space and computation time.

Since simulation efforts are only now giving way to proposed problem solutions, it is too early to draw definitive conclusions. A reprint of a paper describing the application of this simulation code to the evaluation of a triangulation-based short range hazard detection system follows. The reprint is included to illustrate some of the type of output which can be expected when complete simulations of the concepts described herein are implemented.

REFERENCES

1. C.Y. Lee, "An Algorithm for Path Connections and its Application", IEEE Transactions on Electronic Computers, Vol. EC-10, pp. 346-365, September 1961.
2. Fred Lallman, RPI Master's Report, May 1968.

* HORIZONTAL COMPONENTS OF EDGE
 O VERTICAL COMPONENTS OF EDGE
 X APPROXIMATE CENTER OF * & O



STATION 1. PRO-METER CYLINDRICAL ROLLER AT 20 METERS

- * HORIZONTAL COMPONENTS OF EDGE
- O VERTICAL COMPONENTS OF EDGE
- X INTERSECTIONS OF * & O

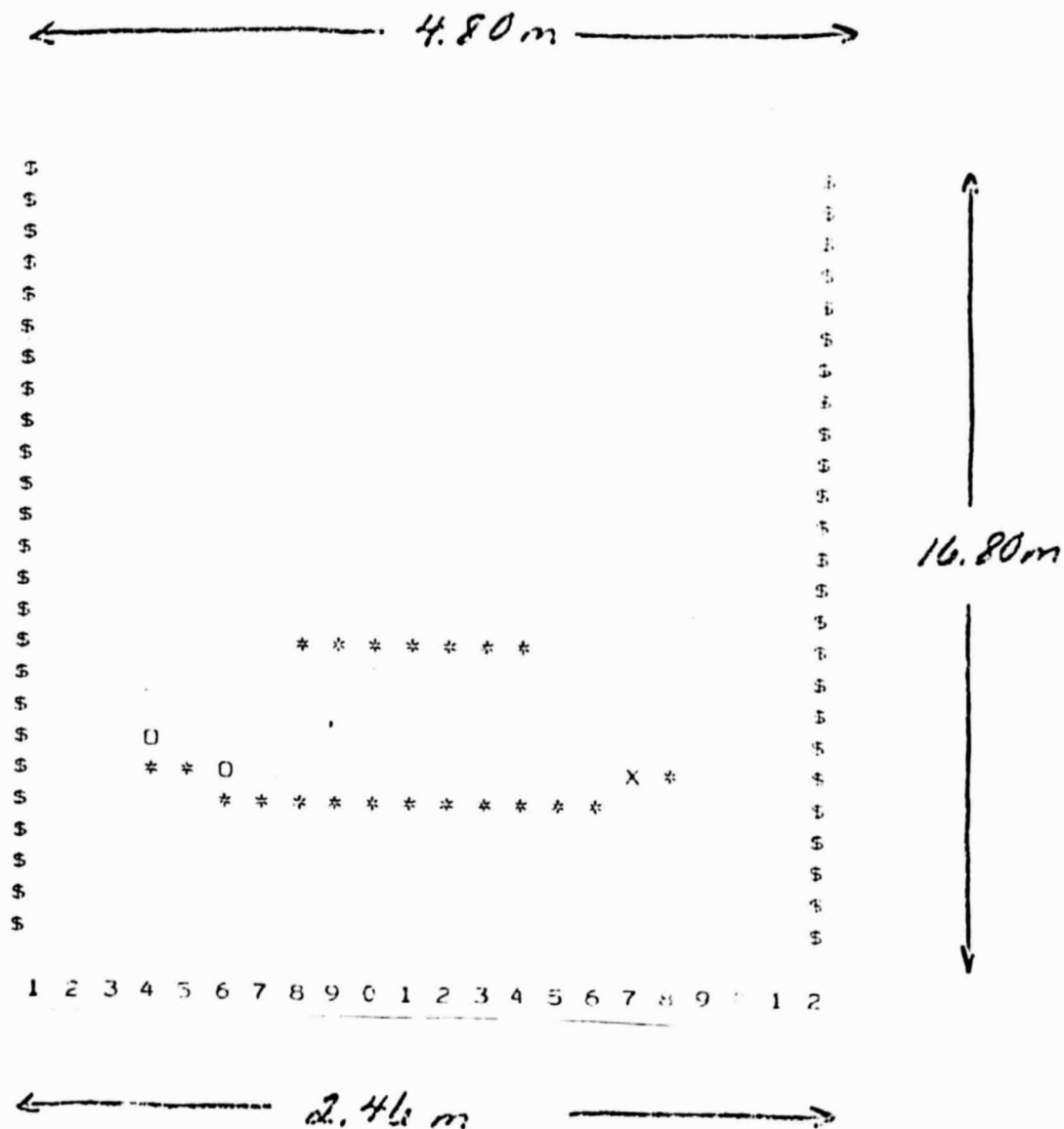


FIGURE 2. TWO-METER GRAPH AT 20 METERS

* HORIZONTAL COMPONENTS OF EDGE
 O VERTICAL COMPONENTS OF EDGE
 X INTERSECTIONS OF * & O

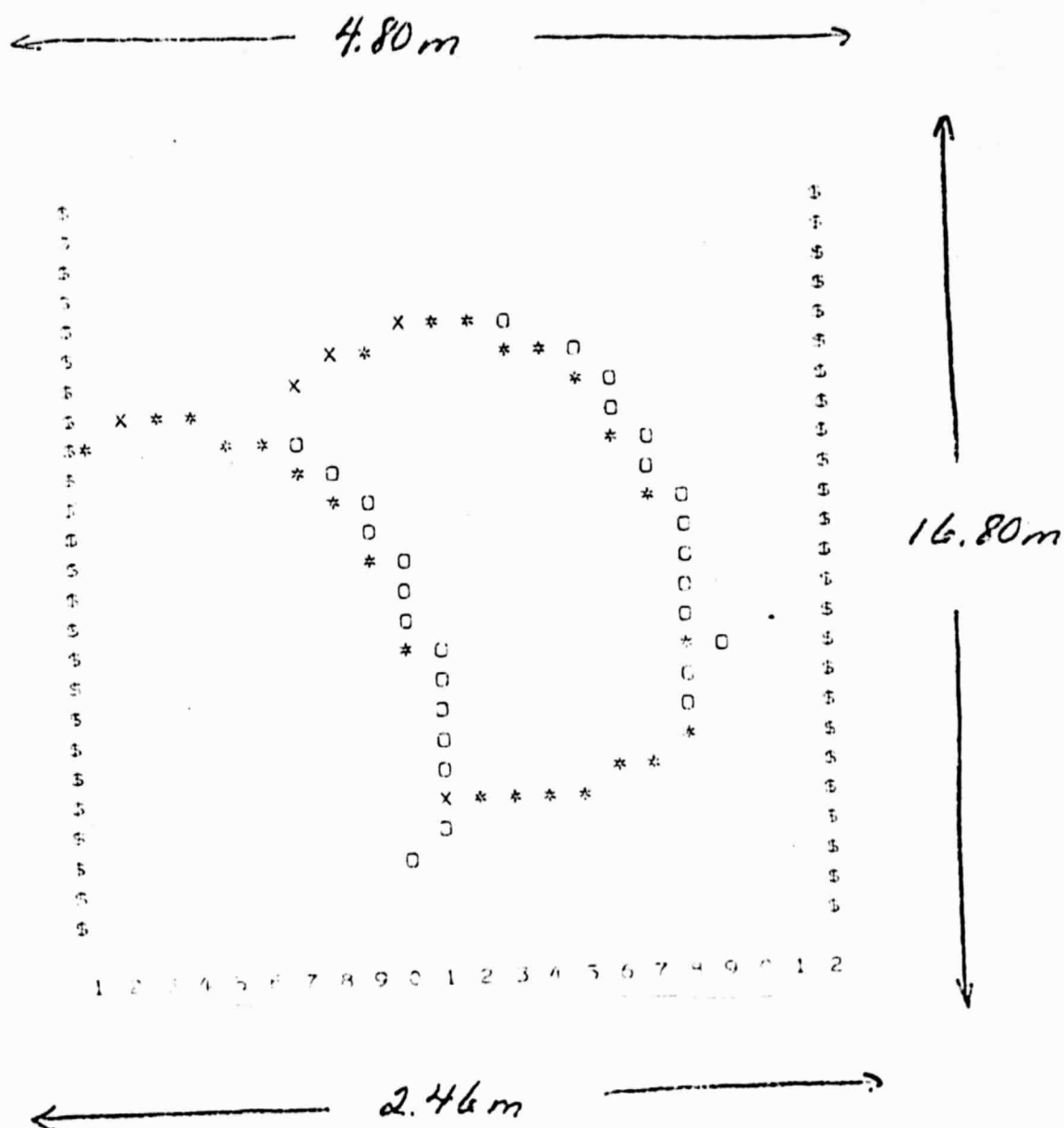


FIGURE 3. TWO TWO-METER SPHERICAL BouldERS AT 20 METERS

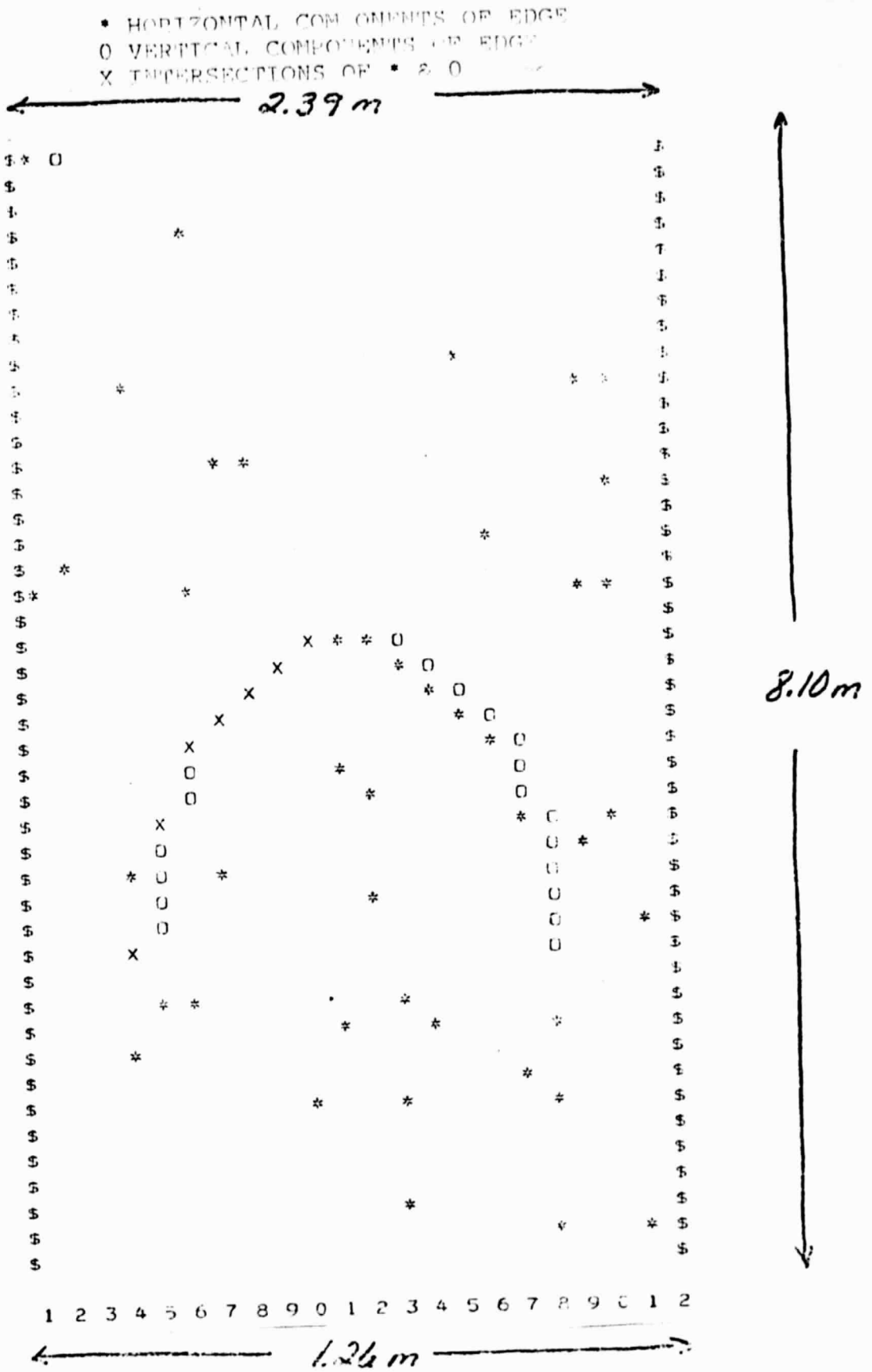


FIGURE 5. ONE-STEP COMPUTATION OF THE 10-MINUTE FLAME INTERFACIAL DISTRIBUTION, 0.2 MPA AND FLATHEAD WITH EQUALLY SPACED

GUIDANCE AND CONTROL OF AN AUTONOMOUS ROVER FOR PLANETARY EXPLORATION

S. Yerazunis, D. K. Frederick and J. Krajewski

Rensselaer Polytechnic Institute
Troy, New YorkORIGINAL PAGE IS
OF POOR QUALITY

A four-wheeled vehicle capable of dealing with irregular terrain features such as might be encountered in unmanned exploration of extraterrestrial bodies has been designed, constructed and tested. Its mobility and maneuverability are such that applications on earth requiring autonomous control may be served by it or a suitable variation. It could also serve as a test bed for artificial intelligence/robotics research. Alternative concepts for terrain sensing and modeling, and path selection algorithms have been investigated. A triangulation-based laser/photodetector path selection system developed by simulation is found to be able to deal with a broad range of terrain features. The path selection system is now in the process of construction and implementation and will permit field evaluation of the overall vehicle system as an autonomous rover.

INTRODUCTION

The very long term interests of man require that a thorough exploration of the planets of the solar system, their moons and the asteroids be undertaken eventually. Although it is likely that man himself will visit or establish himself ultimately on some of these extraterrestrial bodies, economic and technological considerations suggest that unmanned systems must be used during the shorter run.

Considerable knowledge of Mars, Venus, Mercury and Jupiter has been gained by fly-by or orbiter missions and more advanced remote sensor concepts will contribute further to man's understanding of the solar system. However, basic understanding of the chemical, biological, geological, meteorological and physical characteristics of extraterrestrial bodies requires surface exploration. The current Viking missions are intended to meet some of these requirements for the planet Mars.

Despite the historic implications of the Mars Viking program, Viking-type missions are severely limited in scope because of the

restricted sampling range of its ten foot boom with a 120° arc. Thus only a minute fraction of the martian surface will have been scrutinized and a larger but still very small fraction as limited by line of sight will be examined visually. A more thorough exploration is not likely to be effected by increasing the number of such stationary landers because of the large number which would be required and the problem of selecting and reaching precise landing sites where critical measurements can be made. A method for exploring the planet in question in detail and to do so adaptively on the basis of the knowledge being gained is essential.

The scenario for planetary exploration could involve either a stationary lander containing sophisticated and adaptable instrumentation for in-situ analysis or a sample return vehicle. In either case, the scenario must involve sample and/or data gathering devices capable of being relocated over much of the planetary surface, and in the case of sample gathering devices, capable of returning to the lander site. In order that such missions can be executed in a reasonable time of the order of several months to perhaps a year, such sample or data gathering devices must have a high level of both mobility and automatism.

The mobility requirements as expressed in terms of characteristics such as the maximum slope which can be climbed or descended, the maximum boulder which can be negotiated without avoidance, the ability to transverse depressions and very rough terrains, etc., has a direct bearing on the availability of paths to the desired sites. A vehicle of limited mobility may require an inordinate length of time and distance traveled to reach the target. Indeed, in some circumstances, the vehicle may not be able to reach the target. As the vehicle's mobility is increased, it will be able to deal effectively with increasingly difficult terrains. More paths to target will be available and the opportunity for selecting more optimal paths will be increased. Thus, one major research objective should be aimed at developing and evaluating alternative concepts of relocatable devices capable of serving a stationary lander or sample return mission.

Of equal importance to advanced exploration missions is the level of automatism which can be achieved. The decision for the vehicle to follow one path or another towards its destination must be provided by some path selection system comprised of appropriate terrain data

sensors, terrain modeler and path selection algorithm. The character and capabilities of such a system must be appropriate to the objectives of the mission. A low level path selection system will have to be biased conservatively to minimize the risk of an unperceived hazard in the vehicle's path. Thus many, perhaps all, acceptable paths towards the target may be excluded. The effect of a low level detection system is, in fact, to reduce the vehicle's mobility. As a minimum, the path taken towards the destination will be lengthier and the range of the exploration will be reduced. In the other extreme, the vehicle may become immobilized. On the other hand, a higher level, more sensitive, more perceptive path selection system will identify a larger fraction of the passable paths and will permit selection of those directions most compatible with the mission goals. Thus a second major research objective is the development of efficient path selection systems for the safe relocation of a rover.

The research program⁽¹⁾ aimed at these two major objectives is applicable not only to extraterrestrial exploration but to robotics applications on earth where hostile environments and special circumstances may exclude either direct or remote manual control. The major emphasis of this paper is on the rover and the path selection system selected for immediate implementation.

THE RENSSELAER ROVER

By virtue of its design the vehicle has a very high mobility and maneuverability, Ref. 1 and 2. In its deployed state, Figure 1, it has a stable stance allowing it to traverse very irregular terrain. The configuration of the struts serving the individually-driven wheels permits this vehicle to be collapsed into a compact space, Figure 2, from which it can be deployed automatically. The struts, which are driven separately by torsion bars, can be used to raise or lower the payload compartment as required and to orient it fore-and-aft with respect to the horizontal. The front wheel wagon steering insures that all four wheels will be in contact with the terrain for all but the most severe surface irregularities. It also permits a sharp turning radius such that in the extreme case, the vehicle can turn about a center through the rear wheel axles. The vehicle is able to deal effectively with a broad range of slope situations and discrete obstacles.

Perhaps the most outstanding feature of the design is that this vehicle can recover from the situation in which both front wheels fall over the edge of a crevasse or a deep crater. For all other vehicles which have been proposed, such an event would be catastrophic and would terminate the mission. That is not so with this concept.

(1) Faculty participating in the overall research program are: Profs. D.K. Frederick, D. Gisser, G.N. Sandor, C.N. Shen and S. Yezanis.

Because of the unequal lengths of the front and rear struts and the torsion bar system, the front and rear wheel assemblies can be reversed and the vehicle can withdraw safely from the hazard. This same maneuver can be used to extricate the vehicle from a "box canyon" or equivalent terrain feature in which there is insufficient room for the vehicle to turn itself around and from which it may not be able to back out. Previously proposed vehicles would also fail in this instance.

The vehicle has been refined to the point where it can serve as an exceptional test bed for the evaluation of alternative path selection systems. In this sense it is a valuable asset for exploring artificial intelligence or robotic aspects related to a machine seeking an acceptable path to a prescribed destination, an objective not necessarily restricted to extraterrestrial exploration.

In addition to the mechanical and propulsion systems, the rover is equipped with electronic four-wheel speed controls to permit effective steering, attitude and heading gyroscopes, position sensors for all major strut components, and a two-way telemetry link to an off-board mini-computer to provide the necessary vehicle data for guidance and control. All that remains is the implementation of the hardware and software required for an operating path selection system.

PATH SELECTION SYSTEM SIMULATION

The path selection system required to guide an autonomous vehicle must include: terrain sensor or sensors hardware, procedures for interpreting the data, and an algorithm for selecting safe paths on the basis of the data. The best combination of hardware and software will depend on the details of the mission and the dynamical and mobility characteristics of the vehicle or robot. An optimization of these requirements through an iterative process of constructing and evaluating specific hardware and software will be inordinately expensive and tedious and is not likely to be optimal. A digital computer simulation has been developed which can be used to screen all conceivable systems, Ref. 3 and 4. The simulation can "create" a very broad spectrum of terrains possessing such large and small scale details as desired. The pitching, heaving and rolling of the vehicle can be simulated and their effect on the terrain sensor data can be evaluated. The terrain sensor can be simulated to reflect both the error due to the motion of the sensor as a result of vehicular dynamics and the inherent sensor measurement errors. Proposed terrain modelers and path selection algorithms can be analyzed, evaluated and modified. When these considerations are taken all together, a first but meaningful appraisal of the strengths and weaknesses of proposed hardware systems can be obtained. Its application to a specific path selection system is described later in this paper.

ALTERNATIVE TERRAIN DATA GATHERING CONCEPTS

Efforts in developing alternatives for the gathering of terrain data have been focused on:

(a) a range-pointing angle concept and (b) a triangulation concept.

An in-depth study of the use of range-angle pointing data for terrain modeling and hazard detection has been on-going for several years. This phase, which has resulted in numerous publications, Ref. 5, 6, 7, 8, 9, 10, has focused on the mid-range problem from 3-30 meters. Methods have been developed for interpreting these data to obtain estimates of the terrain gradients and to detect discrete objects whose contours deviate from the main terrain. Edge detection and edge enhancement techniques have been developed which provide complete outlines of boulders, ridges, craters and crevasses provided that a sufficiently high data density is available. Current efforts are concentrating on the problem of reducing the data requirements without sacrificing the effectiveness of the interpretation. These studies are concerned with the data density in both time and space and to the implications of inherent sensor errors and errors due to the motion of the sensor as a consequence of vehicular dynamics.

As an alternative, a short range (1-3 meter) system based on triangulation has also been investigated. Indeed the latter system has been selected for implementation on the Rensselaer Rover. The concept is illustrated in Figure 3 in which are shown a laser beam along one pointing angle and a photodetector along a second pointing angle. The existence of a reflecting surface, i.e., terrain within the zone of intersection, will be sensed by the photodetector. In principle, any number of lasers and photodetectors can be deployed to obtain terrain surface data to any desired density and discreteness. This information can then be used as the basis for modeling the terrain and making path selection decisions.

From a terrain modeling point of view, the range-pointing angle and triangulation concepts are equivalent. That is, both concepts provide the same type of data in that the terrain surface is concluded to lie along a line segment of some length and angular orientation. However, the two concepts involve different technical obstacles in their implementation. The uncertainty of locating the terrain surface along the line segment using the range-pointing angle concept is determined by the ability of instrumentation to measure time-of-flight with possibly weak return signals and in the presence of undesired reflections. As one's objective in hazard detection focuses more on the short-range aspect, the time-of-flight measurement becomes increasingly difficult due to the need to measure extremely short time intervals. On the other hand, the uncertainty related with terrain location by triangulation is controlled by the geometrical relationship of the laser and the detector and the cone-of-vision of the latter. By using overlapping detectors and by scanning with a high frequency laser, the uncertainty can be made extremely small for the short range. However, the triangulation system begins to suffer inherent and significant uncertainty in long range applications. Thus, hardware systems based on range-pointing angle data look more attractive at longer ranges whereas the triangulation concept is far more favorable at short range.

Given the objective of demonstrating a minimal level of autonomous roving capability, it was concluded that a path selection system based on the triangulation concept would be implemented.

THE PROPOSED PATH SELECTION SYSTEM

As noted earlier, a path selection system consists of a sensor(s) to gather the data, a terrain modeler to process the data into a proper form, and a path selection algorithm to employ the modeled results with the objective of defining guidance commands. The path selection system which has been chosen for hardware and software implementation consists of two lasers scanned azimuthally along fifteen positions equally spaced at 10° to provide a 140° field of view. One photodetector possessing a 9.6° cone of vision will also be scanned over the same azimuthal angles. The two lasers will be located at a height of 1.5 meters at elevation angles of 43° and 46° whereas the photodetector at the 0.75 meter height will have an elevation angle of 62° , Figure 3. These initial design parameters are specified on the basis of the simulation studies completed to date. The mast on which the lasers and the photodetector are to be mounted has been constructed to provide up to 6 azimuthal 140° sweeps per second. The instrumentation mounting arrangements are such that the lasers can be scanned in elevation as well as azimuth and that additional photodetectors can be added as desired. Finally, the mast configuration will allow for significant adjustment of the geometric parameters so that the researchers will have considerable flexibility in studying more sophisticated triangulation-based alternatives.

Central to the task of demonstrating and evaluating this concept during the late spring of this year has been the path selection system simulation effort. It has fallen on this group to screen a number of design concepts and to synthesize a specific alternative satisfying the basic requirement that the rover will not pursue a path which will abort the mission and that if a safe path to the specified target exists the rover will eventually detect it. Although the long-term objectives call for a high degree of discrimination on the part of the system to minimize the misinterpretation of safe alternatives as hazardous, the studies completed to date have defined a minimum but feasible system.

The path selection system simulation, Ref. 4, has the capability of simulating the performance of a broad range of surface rover concepts, alternative data gathering concepts, data processors i.e. (terrain modelers) and path selection algorithms on a terrain selected by the user. The terrain can have large scale features as well as fine detail. Inherent sensor errors can be simulated along with those sensor errors due to the dynamic motion of the rover as it moves over highly irregular terrain and rubble. Thus, the simulation affords the users the opportunity to appraise alternative hardware and software concepts conveniently.

In the case at hand, the simulation was used to develop the design parameters specified above. The anticipated behavior of the selected system

is shown on Figures 4 through 8. Note that the design parameters are set to detect a positive hazard (boulder or step) or negative hazard (crater or trench) in excess of approximately $\pm 12''$ from the plane defined by the attitude status of the vehicle. With the single detector, this requirement is equivalent to setting the maximum gradient to $\pm 12^\circ$. Parenthetically, it might be noted that the 12° gradient is far lower than the actual slope climbing capability of the Rensselaer Rover. Thus this system will rule out potentially passable paths because of its inability to discriminate between slopes and discrete obstacles.

Shown in Figure 4 are the results of three simulations as applied to a boulder-crater field superimposed on a flat base using the single laser-single detector concept described earlier assuming the absence of noise due either to inherent sensor limitations or the pitch or roll vehicle motions. The proposed path selection system is found to be quite effective in dealing with this problem. Also shown in Figure 4 is a simulation of this system with vehicle motion noise effects equivalent to fluctuations of $\pm 5^\circ$ in pitch and $\pm 10^\circ$ in roll at the contact points of the wheels. At these noise levels, the path selection was unaffected.

The noise parameter referred to above is intended to account for the vehicle motion caused by terrain features which are too small to model on an individual basis. Random fluctuations in the pitch and roll angles are generated and then added to the vehicle's attitude as determined by the slope of the deterministic terrain under the vehicle. These random fluctuations are computed by entering a sequence of uniformly distributed random numbers into a second-order low-pass digital filter whose damping ratio and undamped natural frequency are representative of the vehicle's dominant mode. The purpose of the filter is to simulate the smoothing effect of the vehicle's suspension system. Roll and pitch are treated separately, with different random sequences. For example, using an unfiltered random sequence uniformly distributed over ± 10 degrees resulted in filtered angles having a standard deviation of ± 3.74 degrees and extreme values of ± 9.0 in the pitch direction. Hence, the excursions in the attitude of the mast and laser-detector combination are somewhat less than the unfiltered fluctuations which are assumed to exist at the wheel contact points. The standard deviation and the extreme values for other levels of vehicle dynamic noise would be proportional to these for 10 degrees.

Also shown in Figure 4 are simulations involving the two-laser system scheduled for implementation with noise levels of 10° and 15° in both pitch and roll. The performance of the system continues to be effective despite the high noise levels. However, it is clear that as the noise level due to vehicular dynamics and terrain irregularities is increased, a point will be reached eventually at which the effectiveness of the path selection system will be degraded. This question has not been fully explored yet because as will be described below noise effects are far more significant in terrain situations involving surface undulations than on flat base terrains.

Shown in Figure 5 are simulations involving a terrain described by sinusoidal functions. It should be noted that for a sinusoidal terrain of 6 meter period and 0.20 meter amplitude in the absence of noise that the path selection system is able to direct the vehicle in a straight line fashion between the initial point and the target destination. However, an increase of the amplitude to 0.3 meter forces the one laser hazard detection system to depart significantly from the straight line path and to meander toward the target. Although the target is reached eventually a considerably larger distance traveled is involved. The path selection system can be improved by adding a second laser at an incremental elevation of 3° . This modification has the effect of providing additional information which allows the path selection system to take a somewhat more direct route toward the target. However neither system can achieve a direct route for an amplitude of this magnitude. Increasing the amplitude to 0.33 meters while retaining the period at 6 meters, causes both the one and two-laser systems to prescribe an even more tortuous path. At an amplitude 0.4 meters, the system is unable to contend with the situations and fails to make progress towards the target. The simulations shown in Figure 5 highlight a major weakness in this simple hazard detection system, namely, its inability to distinguish between a slope and a discrete obstacle. The rover found itself obliged to turn from the direct path at critical points where the sensor was detecting the existence of a moderate slope in excess of the 12° limit imposed by the assumed sensor system. It had to take on a direction such that the gradient to be encountered would be within the specified tolerance limits. This is not necessarily a fatal flaw since the rover was able to select a trajectory either up or down hill which would be satisfactory. But it did so at the penalty of taking an unnecessarily long trajectory.

The consequences of dynamic noise are far more significant with respect to rolling terrain situations than in the case of the flat terrain on which a variety of boulder and crater obstacles are superimposed. This behavior is shown in Figure 6 in which the one-laser and the two-laser systems are tested in a .3 meter amplitude, 6 meter period sinusoidal terrain with noise due to vehicle dynamics equivalent to 10° in pitch and 10° in roll. In order to compare the two alternatives, the same seed was used to generate the random numbers which serve as the basis for calculating the noise. Thus, both systems were tested against the same exact sequence of dynamical motion. Both simulations failed to the extent that extreme meandering and confusion is observed. It cannot be concluded that the target would not have been reached ultimately because the simulations were automatically terminated on the basis of a time constraint. However, what is important to note in this comparison is that the two-laser system had no observable superiority over the one laser system in the case of this rolling terrain at this level of dynamical noise. Also shown in Figure 6 is the performance of the two laser system with vehicle dynamics noise reduced to 5° in pitch. Although a meandering path was followed, the system would ultimately lead the rover to the target.

Shown in Figure 7 are the results of three simulations all involving a rolling terrain described by a .25 meter amplitude, 6 meter period sinusoidal surface. Two of the simulations compare the effectiveness with which the one- and two-laser systems could deal with this rolling terrain situation in the presence of 10° pitch, 10° roll dynamical motion. Neither simulation proved to be particularly effective although the failure to reach the target is again a consequence of terminating the simulation rather than a fundamental inability to achieve the target ultimately. Nevertheless, in the case of this level of dynamical noise it is clear that the path selection system is forcing the rover into very substantial meandering and is therefore not considered effective for both the one- and two-laser systems although the latter appears stronger. However, the third simulation involving dynamical noise levels of only 5° in pitch but with the 10° roll retained showed that the two-laser system was able to take a relatively direct route from the starting point to the final destination. This suggests therefore that in the design of an autonomous rover a significant impact on the effectiveness of hazard detection and path selection systems can be obtained by careful vehicular design which minimizes the effect of dynamical noise upon the sensing devices. Another way of looking at the significance of these simulations is to note that it is the sum of the gradients representative of the physical terrain situation and of the noise effects which determine how well the path selection system will perform for a given vehicle. On the basis of the data at hand, it can be concluded that even with a 10° pitch noise due to dynamical motion that there would be some rolling terrain either with reduced amplitude and/or increased period which could be handled effectively by this system. In effect, the consequences of the noise associated with the dynamical motion is to reduce the mobility of the vehicle by applying a bias required to offset the impact of noise.

Summarized in Figure 8 are the results of three simulations in the absence of vehicle dynamics noise in which the boulder/crater field is superimposed on the sinusoidal rolling terrain. The combined terrain features are seen to pose a more serious problem than for either case separately. Case 1 involving the vehicle origin in the upper right hand corner found the vehicle getting itself into an awkward position in which a considerable amount of maneuvering was required before a good trajectory toward the target could be defined. The discontinuities in path which are shown are a consequence of the simulation program which applies when the vehicle finds itself in an impossible situation. The algorithm calls for the vehicle to back up 1 meter. As far as the simulation is concerned this backup is instantaneous and discontinuous. Case 2 involving an initiation point in the upper left hand corner for a two-laser system proceeded rather well to the target whereas the corresponding path for the one-laser system encountered difficulty near the target and a considerable meandering before reaching the target. Also shown for comparison in Figure 8 is the path selection process for the boulder/crater field on a flat plane. It can be seen that the effect of the rolling terrain is to deny to the vehicle the most direct route to the target. However, the final simulation shown involving a

5° in pitch and 10° in roll vehicle dynamics noise closely parallels the path of the noiseless flat terrain case. It would appear that in this case, the noise led to a fortuitous selection of path.

Other simulations not reported herein have been conducted which suggest ways in which the system could be modified to deal more effectively either with the discrete obstacle such as boulders, craters, trenches or with slope characteristics. The tendency to interpret passable slopes as impassable can be reduced increasing the cone of vision of the detector. However, the effect of this action is to increase the size of the positive or negative discrete hazard to be interpreted as passable. A decrease in the cone of vision of the detector will permit smaller discrete obstacles to be detected but at the penalty of defining lower acceptable slope thresholds. The design parameters which have been selected as of this date represent what is believed to be the best compromise for the purpose of demonstrating and evaluating this kind of a system in hardware.

As noted earlier, the problem of noise due to vehicle dynamics has the effect of biasing the path selection decisions conservatively. The pitching or rolling motion of the vehicle provides false information which is interpreted as a vehicle hazard. It is also possible for the dynamical noise to give a false indication that a hazard is not present even though it really is. The latter does not prove to be significant because subsequent scans will disclose the existence of a real hazard, even though it may be overlooked on an individual scan. The reverse is not true; when a path is deemed to be blocked because of the dynamical noise, the path selection algorithm treats it as being blocked and not only directs the vehicle otherwise but retains in its memory that that path is blocked. Consideration is being given to incorporating memory into the terrain modeler and path selection algorithm so as to reduce the false identification of hazardous paths. Such a system should provide a basis for alleviating the type of erratic behavior shown in Figures 6 and 7.

The present path selection system has one additional major fault to which attention is being directed. Specifically, past researchers, Reference 11, have shown that a particular terrain feature may or may not be a hazard depending upon the main terrain characteristics on which the feature is located. Thus in the ultimate, it will be necessary to relate the state of the terrain, as defined by the attitude information provided by the attitude gyroscope mounted on the vehicle to the data being provided by the hazard detection sensors. One possible solution is to implement a higher level triangulation-based system which involves elevation as well as azimuthal scanning of the laser and an increased number of detectors with smaller cones or zones of vision. The effect of this type of a system is of course to decrease the coarseness of the information. Provided that a sufficiently fine mesh is obtained, pattern recognition techniques can be used to obtain a much more detailed and informative impression of the nature of the terrain in the path of the vehicle. The information gained in such a system could be tied to the

vehicle attitude data through appropriate mathematical relationships to provide a more sound decision as to whether the terrain feature is or is not a hazard for the vehicle's particular state.

Alternatively, one could consider using the basic system described herein but replicating it in sufficient number so that only one of the systems would be operational at a given time depending upon the vehicle's attitude. Thus one might have a multi-unit system of the type described herein with the central unit applying to all situations in which the vehicle's attitude is not far removed from horizontal, with the immediately adjacent two units applying when the vehicle's attitude is slightly upwardly or downwardly inclined, and with additional adjacent units applying at greater and greater attitudinal deviations from horizontal. The number of such units would depend on the need for refined terrain information.

Consideration is being given to other systems of intermediate complexity, namely, five 90° detectors overlapped as to produce nine discrete signals in combination with from three to five lasers being scanned azimuthally but with each laser at a very specific elevation. Such an intermediate system can be implemented in hardware and software relatively easily and have the advantage of providing enough added information to give the path selection algorithm a more reliable basis for decision making.

As of this writing, the research program to produce the required hardware, (i.e. lasers, photodetectors, scanning mast, etc.) and to program the software in a IDIOM Graphics-Varian Computer, which is to serve as the data processor, are proceeding vigorously. The rover itself and its on-board control systems and actuators are operational along with the telemetry systems required to transmit data from the vehicle to the computer and vice versa. It is anticipated that all systems will be active in the neighborhood of April 1, and that laboratory and field research will be undertaken shortly thereafter.

CONCLUSIONS

1. A path selection system based on a two-laser/one-detector terrain sensor can be effective in guiding an autonomous rover over terrains whose general slopes are less than $\pm 12^\circ$ and on which are distributed discrete hazards larger than ± 12 inches in the presence of vehicle dynamics noise of the order of $\pm 5^\circ$ in pitch and $\pm 10^\circ$ in roll.
2. The performance of such a system can be increased provided that the state (i.e. the attitude) of the vehicle is taken into account in the interpretation of the sensed terrain data and that additional attitude dependent sensor units are added.
3. Terrain sensors based on triangulation provide a basis for developing short-range path selection systems capable of dealing with very complex terrain situations.

ACKNOWLEDGEMENT

The authors acknowledge gratefully the critical contributions of Dr. G. N. Sandor and his student research assistants who designed and constructed the rover and its associate electro-mechanical systems.

The technical guidance and recommendations provided over past years by Dr. G. Payne and Mr. B. Dobrotin of the Jet Propulsion Laboratory and by Mr. P. Tarver of the Office of Lunar and Planetary Studies of NASA are deeply appreciated.

The authors also acknowledge the generous and extended support of the Office of Lunar and Planetary Studies of the National Aeronautics and Space Administration through Grant NGL 33-018-091.

REFERENCES

1. Rayfield, W.P., and Sandor, G.N., "Design of Roving Vehicle for Mars," Invited Paper, presented at the ASME Design Engineering Conf., New York, N.Y., April 19-22, 1971.
2. Sandor, G.N., "Seven Dangers of Designer Overspecialization and How to Avoid Them By Designer Education," Invited ASME Paper No. 74-DE-35, 1974 Design Engineering Conference, Chicago, April 1-4, 1974, to be preprinted by the ASME in full and to be published in abstract in Mechanical Engineering, Journal of the ASME.
3. Campbell, R.S. and Simonds, R.R., "Path Selection System Development and Evaluation for a Martian Roving Vehicle," RPI Technical Report MP-42, Rensselaer Polytechnic Institute, Troy, N.Y., May 1974.
4. Frederick, D.K., "Path Selection System Simulation and Evaluation for a Martian Roving Vehicle," 6th Annual Pittsburgh Conference on Modeling and Simulation, Pittsburgh, Pa., April 1975.
5. Shen, C.N. and Burger, P., "Stochastic Estimates of Gradients from Laser Measurements for an Autonomous Martian Roving Vehicle," Proceedings of 3rd IFAC Symposium, The Hague, June 1973.
6. Shen, C.N. and D'Angelo, R.P., "Parameter Estimation for Terrain Modeling from Gradient Data," 7th Hawaii International Conference on System Sciences, Hawaii, January, 1974.
7. Shen, C.N. and Thompson, A., "Computer Results of Two-Dimensional Spline Function in Terrain Modeling Optimization," ACM 1975 Computer Science Conference, Washington, D.C., February 1975.
8. Reed, M., Sanyal, P. and Shen, C.N., "A Practical Obstacle Detection System for a Mars Rover," Proceedings of the Milwaukee Symposium on Automatic Controls, March 1974, Milwaukee, Wisconsin.

9. Shen, C.N. and Sonalkar, R.V., "Mars Obstacle Detection by Rapid Estimation Scheme from Noisy Laser Rangefinder Readings," Milwaukee Symposium on Automatic Computation and Control, Milwaukee, Wisconsin, April 1975.
10. Shen, C.N. and Sher, J.S., "Simulation of the Range Data and the Picture Enhancing Scheme for a Mars Rover," ACM 1975 Computer Science Conference, Washington, D.C., February 1975.
11. Shen, C.N., Leung, K.L. and Yerazunis, S., "Classification of Terrain Models for a Martian Vehicle," 6th Annual Pittsburgh Conference on Modeling and Simulation, Pittsburgh, Pa., April 1975.

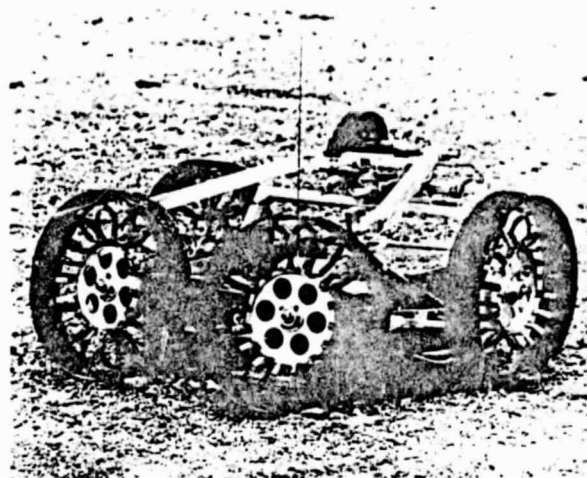


Figure 2. The Rensselaer Rover in its Deployed Configuration

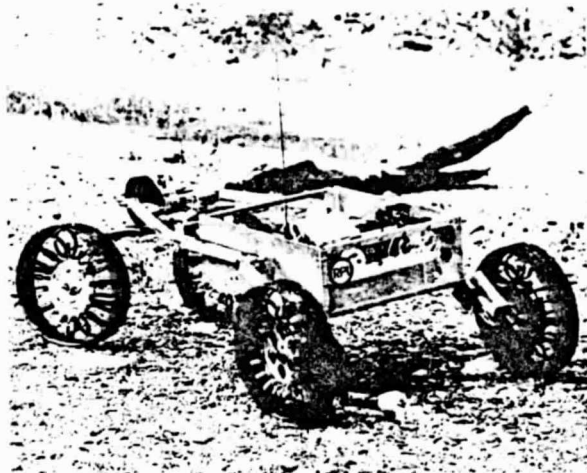


Figure 1. The Rensselaer Rover in its Collapsed Configuration

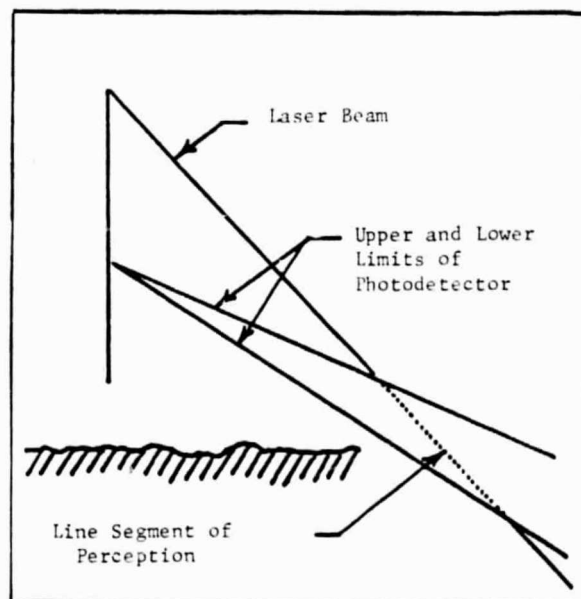


Figure 3
Terrain Detection by Triangulation

ORIGINAL PAGE IS
OF POOR QUALITY

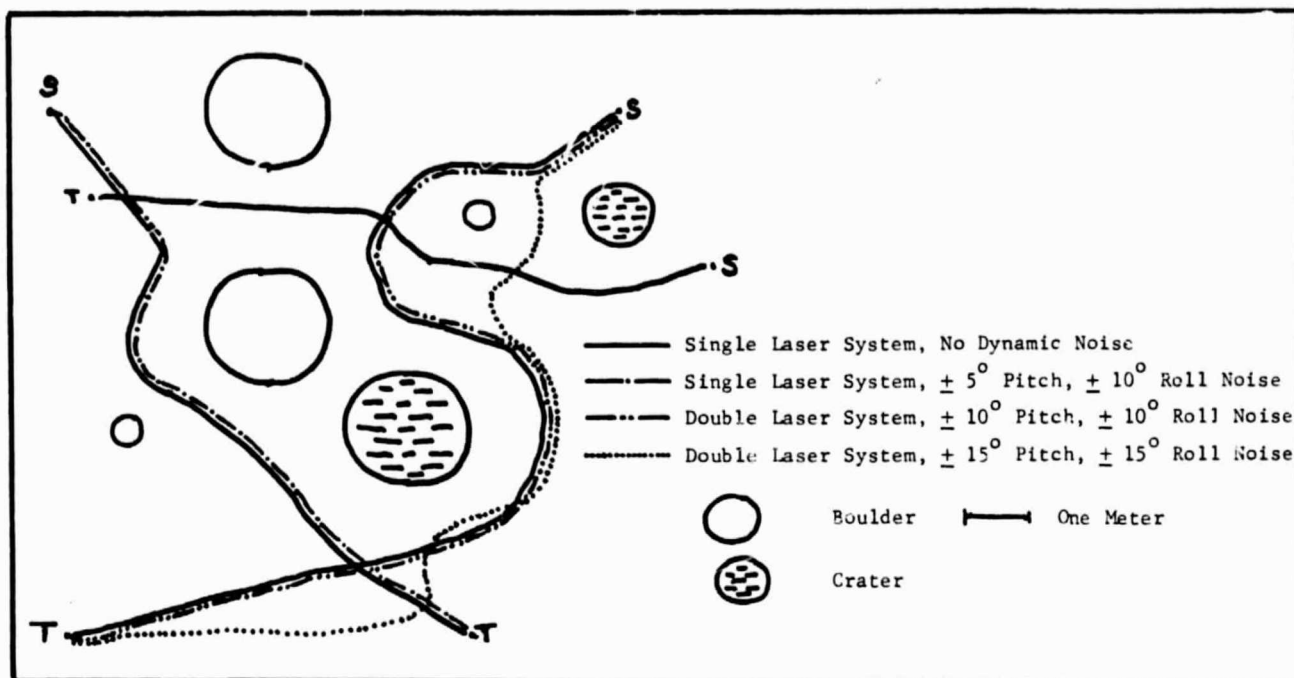


Figure 4. Path Selection Simulation Through a Boulder/Crater Field on a Flat Base Terrain

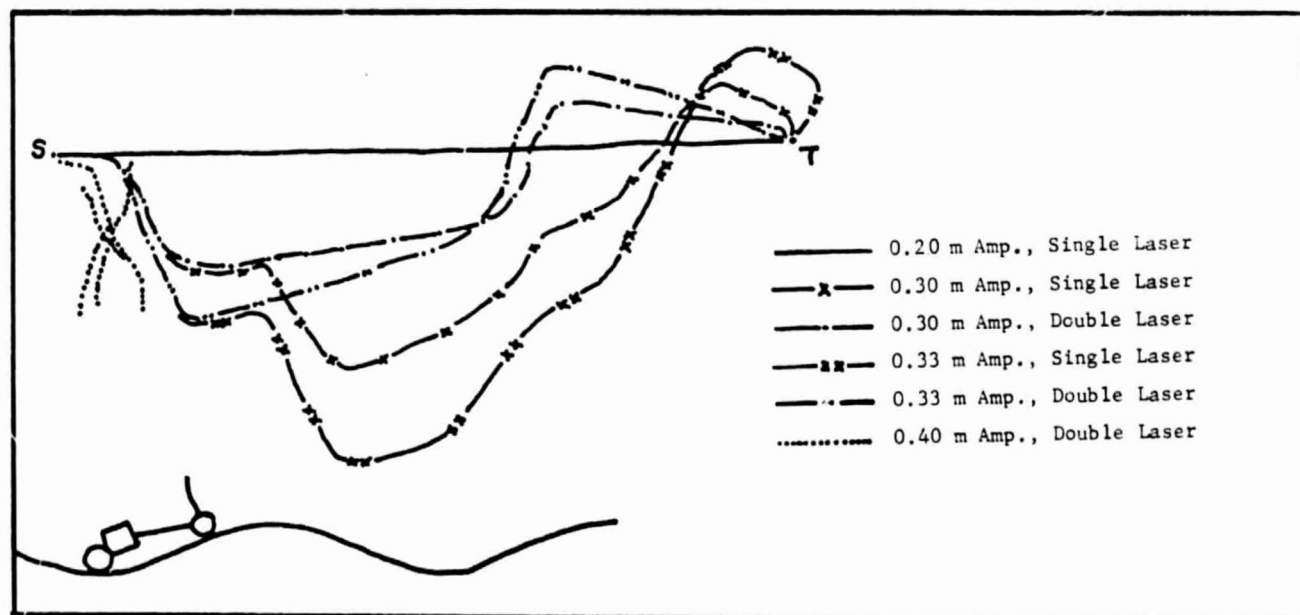


Figure 5. Path Selection Simulation Over a 6.0 Meter Period Sinusoidal Terrain in the Absence of Vehicle Dynamics Noise

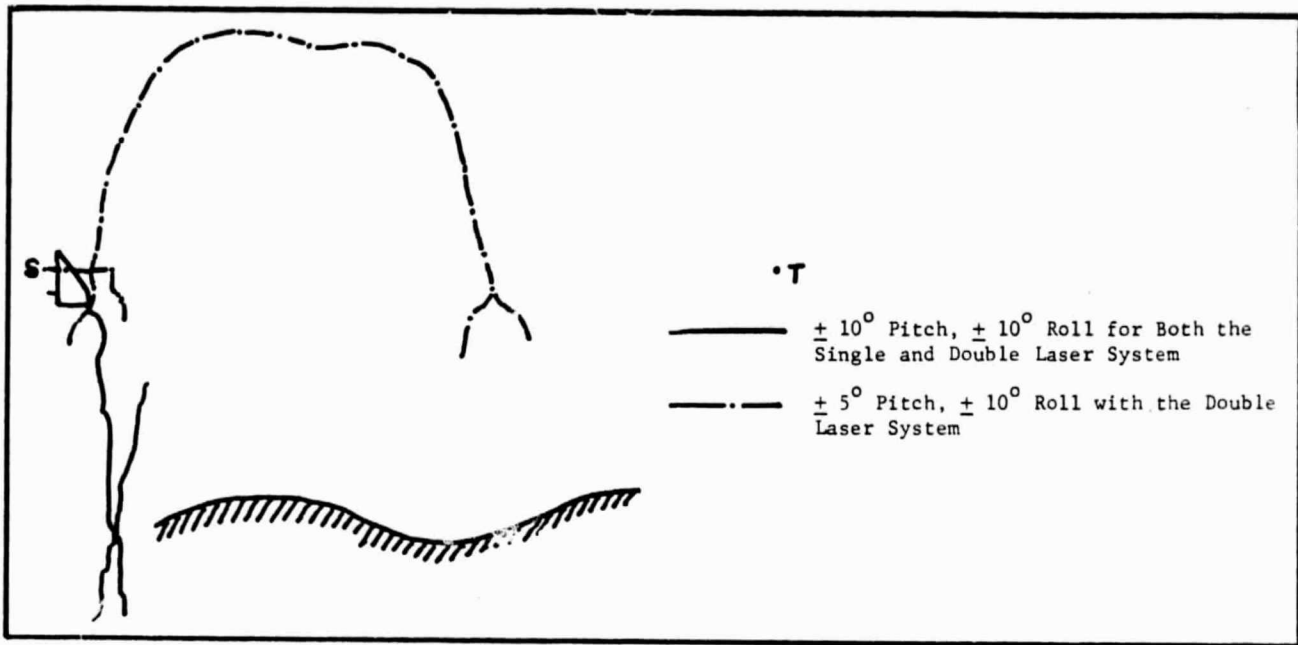


Figure 6. Path Selection Simulation for a Sinusoidal Terrain 0.3 Meter Amplitude and 6.0 Meter Period in the Presence of Vehicle Dynamics Noise

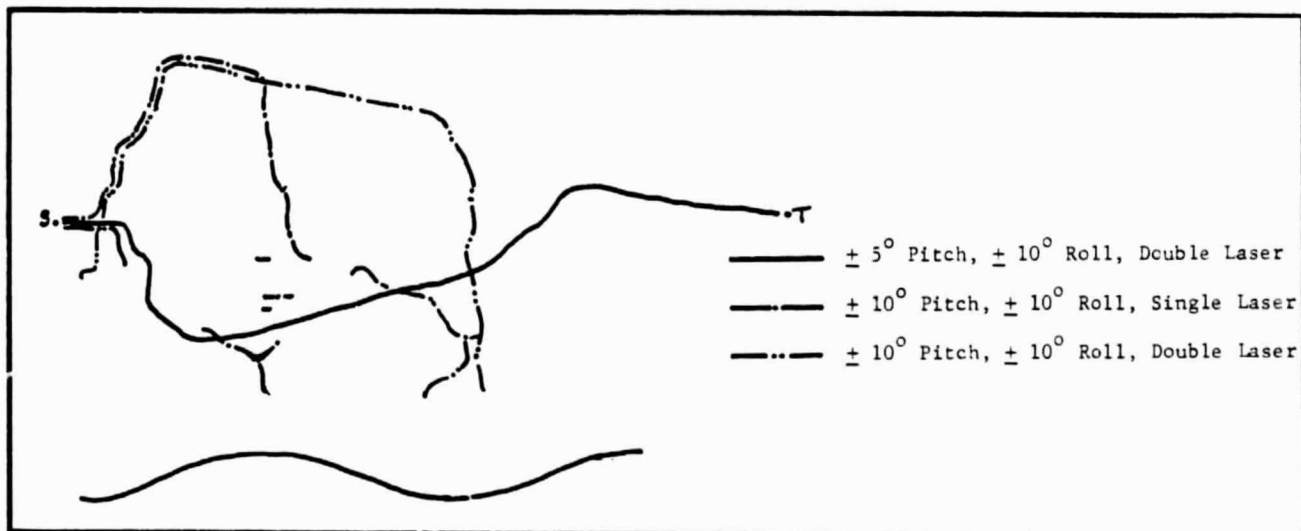


Figure 7. Path Selection Simulation for a Sinusoidal Terrain of 0.25 Meter Amplitude and 6.0 Meter Period in the Presence of Vehicle Dynamics Noise

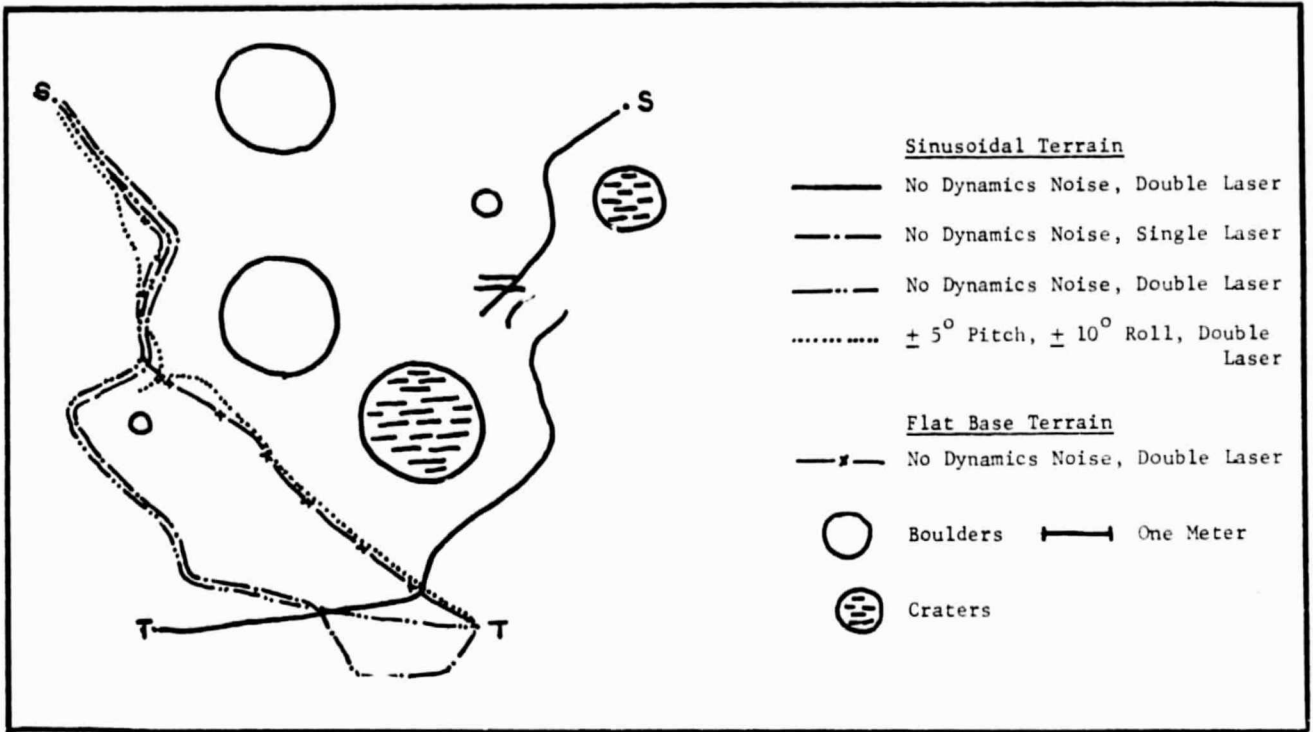


Figure 8. Path Selection Simulation for a Boulder/Crater Field Superimposed on a Sinusoidal Terrain of 0.3 Meter Amplitude and 6.0 Meter Period